



THE UNIVERSITY *of* EDINBURGH

Edinburgh Research Explorer

Formation processes of dunites and chromitites in Orhaneli and Harmanck ophiolites (NW Turkey): Evidence from in-situ Li isotopes and trace elements in olivine

Citation for published version:

Chen, C, De Hoog, JCM, Su, B, Wang, J, Uysal, I & Xiao, Y 2020, 'Formation processes of dunites and chromitites in Orhaneli and Harmanck ophiolites (NW Turkey): Evidence from in-situ Li isotopes and trace elements in olivine', *Lithos*, pp. 105773. <https://doi.org/10.1016/j.lithos.2020.105773>

Digital Object Identifier (DOI):

[10.1016/j.lithos.2020.105773](https://doi.org/10.1016/j.lithos.2020.105773)

Link:

[Link to publication record in Edinburgh Research Explorer](#)

Document Version:

Peer reviewed version

Published In:

Lithos

Publisher Rights Statement:

© 2020 Elsevier B.V. .

General rights

Copyright for the publications made accessible via the Edinburgh Research Explorer is retained by the author(s) and / or other copyright owners and it is a condition of accessing these publications that users recognise and abide by the legal requirements associated with these rights.

Take down policy

The University of Edinburgh has made every reasonable effort to ensure that Edinburgh Research Explorer content complies with UK legislation. If you believe that the public display of this file breaches copyright please contact openaccess@ed.ac.uk providing details, and we will remove access to the work immediately and investigate your claim.



Manuscript Number: LITHOS9129R2

Title: Formation processes of dunites and chromitites in Orhaneli and Harmancık ophiolites (NW Turkey): evidence from in-situ Li isotopes and trace elements in olivine

Article Type: Regular Article

Keywords: olivine; trace element; Li isotopes; ophiolite; chromitite; mantle-crust transition zone

Corresponding Author: Dr. Chen Chen, Ph.D.

Corresponding Author's Institution:

First Author: Chen Chen, Ph.D.

Order of Authors: Chen Chen, Ph.D.; Jan C.M. De Hoog; Ben-Xun Su; Jing Wang; İbrahim Uysal; Yan Xiao

Abstract: Trace elements and Li isotopic compositions of olivine from the mantle-crust transition zone of the Bursa ophiolites (including Orhaneli ophiolite and Harmancık ophiolite) in NW Turkey were measured to constrain the genesis of these dunites and chromitites. A cumulate origin for dunite can be ruled out due to the depletion of incompatible trace elements (Zr, Ti, and heavy rare earth elements) in olivine, instead the chemical signatures point to a replacive origin via melt-rock interaction. The olivine grains in the dunites have lower MnO (0.06-0.15 wt.%), Co (106-137 ppm), Ca (73-323 ppm), and higher NiO (0.23-0.44 wt.%) concentrations than olivine phenocrysts in MORB, suggesting these transition-zone dunites have equilibrated with extremely depleted melts. Additionally, the relatively small $\delta^{7}\text{Li}$ variations of olivine (average $\delta^{7}\text{Li}$ +4.8 to +8.7‰) of the Orhaneli suite indicate the Li isotopic compositions of melts percolating through these dunites are relatively homogeneous. However, the large $\delta^{7}\text{Li}$ variations of olivine (-2.5 to 20.3‰) in Harmancık dunites can be explained by incomplete diffusive equilibration with melts percolating through these dunites, suggesting infiltration happened not long before obduction of the ophiolite. Olivine in chromitites has higher Fo (92.6-94.7) than coexisting dunites, likely induced by subsolidus Mg-Fe exchange between olivine and chromite. The higher chromite contents of the chromitites can also explain the lower concentrations of Sc, V, Co and Zn in coexisting olivine grains. Mixing of depleted mantle-derived melts and boninitic magmas is suggested to induce a compositional shift from the olivine-chromite cotectic line to the liquidus field of chromite, causing the precipitation of chromite and formation of chromitite layers in the dunites. The heavy Li isotopic compositions (+5 to +11‰) of olivine in chromitites and dunites compared to MORB, together with the estimated compositions of parental magmas (Al_2O_3 : 9.8-11.4 wt.%; TiO_2 : 0.22-0.38 wt.%) for the chromitites, indicate an arc-like geochemical affinity, hence a subduction-related setting in which these mantle-crust transition zones formed.

Research Data Related to this Submission

Title: Data for: Formation processes of dunites and chromitites in Orhaneli and Harmancik ophiolites (NW Turkey): evidence from in-situ Li isotopes and trace elements in olivine

Repository: Mendeley Data

<https://data.mendeley.com/datasets/6nwr9d8z78/draft?a=ebf4efdf-b318-4ee5-8fc4-d1d0276533ea>

Formation processes of dunites and chromitites in Orhaneli and Harmancık ophiolites (NW Turkey): evidence from in-situ Li isotopes and trace elements in olivine

Chen Chen^{1,2,3*}, Jan C.M. De Hoog^{4*}, Ben-Xun Su^{1,3,5}, Jing Wang^{1,3,5}, İbrahim Uysal⁶, Yan Xiao^{3,7}

¹ Key Laboratory of Mineral Resources, Institute of Geology and Geophysics, Chinese Academy of Sciences, Beijing 100029, China

² Key Laboratory of Mineralogy and Metallogeny, Guangzhou Institute of Geochemistry, Chinese Academy of Sciences, Guangzhou 510460, China

³ Innovation Academy for Earth Science, Chinese Academy of Sciences, Beijing 100029, China

⁴ Grant Institute, School of GeoSciences, The University of Edinburgh, Edinburgh, EH9 3FE, United Kingdom

⁵ University of Chinese Academy of Science, Beijing, 100049, China

⁶ Department of Geological Engineering, Karadeniz Technical University, 61080 Trabzon, Turkey

⁷ State Key Laboratory of Lithospheric Evolution, Institute of Geology and Geophysics, Chinese Academy of Science, Beijing 100029, China

*Corresponding authors: chenchen2@gig.ac.cn (Chen Chen)

ceesjan.dehoog@ed.ac.uk (Jan C.M. De Hoog)

Dear editor,

We really appreciate the insightful comments on our submission by you and the two reviewers, which gave us the opportunity to clarify several important aspects of our manuscript. We revised the manuscript according to the comments, with the major changes as follows:

1. Figure 9 and 12 are modified, and the corresponding explanations are provided in the figure captions. Previous Figure 6 and Figure 10 are removed from the revised version. The related sentences in the text are revised accordingly.
2. The “Highlights” have been shortened.
3. Unrelated references have been removed from the revised version and the total number of references is now 79.

In addition, all editorial comments by the reviewers have been incorporated in the revised version, and point-to-point responses to more detailed comments are listed below. All changes have been highlighted in yellow in the revised manuscript.

We hope you find this revised version of the manuscript suitable for publication in *Lithos*, and look forward to any further comments.

Best regards,
Chen Chen and co-authors

Detailed responses to comments (our responses in red font)

Editor's comments:

Both reviewers find the topic of interest and suggest minor revisions. Based on the two favorable reviews and my own reading of the paper, I am pleased to inform that your paper should be acceptable for publication in the journal after suitable revision is made following the reviewer comments.

1. Highlights 1-3 are too long. Each bullet point of highlights should be no more than 85 characters, including spaces.

Reply: The highlights have been shortened.

2. The number of references exceeds the *Lithos* maximum of 80. Please reduce the number of references.

Reply: Unrelated references have been removed from the revision and reference number is now 79.

3. Submit data tables 1 to 3 as supplementary material for online publication.

Reply: Data tables 1 to 3 have now been prepared supplementary material for online publication.

Reviewer #1:

The authors have made in-situ analyses on trace element and Li isotopic compositions of olivine from dunites and chromitites in Orhaneli and Harmancik ophiolites (NW Turkey) to unravel the genesis of the host rocks. The data were clearly reported; the manuscript is well structured and fully referenced. Based on the data, the authors made reasonable discussion for the genesis of the dunites and chromitites.

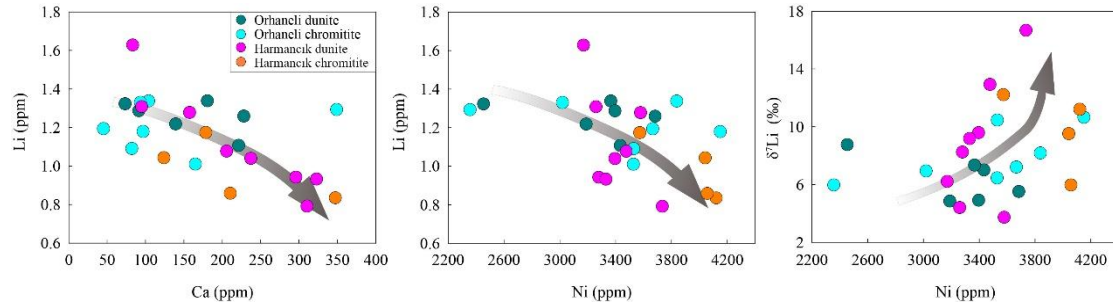
I have only minor comments on the manuscript as shown below:

1. The authors proposed that dunites have equilibrated with the depleted melts as revealed by trace element compositions of olivine in dunites from both Orhaneli and Harmancik ophiolites. But the large $\delta^7\text{Li}$ variations among individual samples and the negative correlation between Li concentrations and $\delta^7\text{Li}$ values for the Harmancik dunites indicate the incomplete equilibrium of Li isotopes between dunites and incorporated melts shortly before obduction and exhumation. As Li has higher diffusivity than other trace elements in olivine, these observations implicate that they belong to different stages of melt percolation. In the manuscript, I suggest that the authors clarify the temporal and original relationship of percolated melts responsible for the formation of dunites, and the formation of chromitites, and the large $\delta^7\text{Li}$ variations among individual samples, respectively.

Reply: Some Templeton experiments found that the isotopic gradients dissipate slower than gradients in the parent element. Richter et al. (2014) reported that very large lithium isotopic fractionations persisted after the lithium concentration had become effectively homogenized during diffusion process, suggesting that it still takes longer for the isotopic composition to become uniform compared to the time it takes for diffusion to homogenize the total lithium concentration. Thus, we can observe the Li element and other trace element concentrations of olivine in dunites from Harmancik ophiolite are equilibrated with the infiltrating melts, whereas the $\delta^7\text{Li}$ variations of olivine are large, which is caused by incomplete equilibrium of Li isotopes between dunites and incorporated melts. Therefore, these observations are the same stage of melt percolation, and not belong to different stages of melt percolation. In the revision, a detailed discussion has been added to Section 6.4.

2. The authors could identify whether there is any correlation between the concentrations of other trace elements (or other geochemical signatures, e.g., Fo) and Li (or $\delta^7\text{Li}$ values) in olivine. It may have some implications for the histories of melt percolation.

Reply: According to the reviewer's suggestion, we plotted the figures of concentrations of other trace/major elements and Li concentrations/ $\delta^7\text{Li}$ values, found there are relatively apparent correlations between Li concentrations/ $\delta^7\text{Li}$ values and Ca concentrations or Ni concentrations of olivine, which is also caused by melt-rock interaction. This conclusion is consistent with this paper. Because the reviewer pointed that the manuscript has many figures and suggested deleting or merging some of them, we do not show these figures in the manuscript.



3. The authors ascribed the large heterogeneity of olivine Li isotopic compositions in dunites from the Harmancik ophiolite as the result of disequilibrated Li diffusion during melt percolation. The diffusive addition of Li from melts in short periods can induce relatively higher Li concentrations and lower $\delta^7\text{Li}$ values in some samples. However, for samples with heavy Li isotopic compositions ($\delta^7\text{Li}$ as high as 20‰), the disequilibrated Li diffusion seems not accountable, as Li concentrations (as low as 0.7 ppm) are markedly lower compared to MORB or IAB (meaning that the diffusive loss of Li from dunites to melts is difficult). In Figure 9, the authors illustrated that these high $\delta^7\text{Li}$ values may result from partial melting (inherited from source rocks, depleted peridotites?). For this point, more discussion is needed to make it clear.

Reply: In the olivine of dunite from ophiolites, many studies have reported that there is a negative correlation between Li concentrations and $\delta^7\text{Li}$ isotopic compositions and the Li concentrations of olivine with high $\delta^7\text{Li}$ values can be similar to or slightly lower than those in the normal mantle (1.0-1.8 ppm), which can be explained by the interaction between melt and peridotite. For example, in the dunite from Trinity ophiolite, Lundstrom et al. (2015) observed that the $\delta^7\text{Li}$ values and Li concentrations olivine vary from -5 to 21 ‰ and from 0.6-1.2 ppm, respectively, and Li concentrations vary widely and negatively correlate with $\delta^7\text{Li}$ for olivines. These features could reflect mineral interaction with hydrothermal fluids where Li partitioning behavior changes with temperature. Su et al. (2016) reported that the olivine in the dunite from the Luobusa ophiolite have Li concentrations (Li isotopic compositions) varying from 0.30 to 0.60 ppm (~10 to 20 ‰). The trend of higher $\delta^7\text{Li}$ with decreasing Li concentration is also attributed to the diffusion from melts to the surrounding peridotites (Su et al., 2016).

The olivine grains dunites from the Harmancik ophiolite have Li concentrations and Li isotopic compositions varying from 0.7 to 1.9 ppm and from 2.5 to 20.3‰, the ranges and patterns comparable with those in Trinity dunite (Lundstrom et al., 2015), indicating the result of melt-rock interaction process. In the revision, the related discussion has been added to Section 6.4.

Sorry for the confusion, we have deleted the “partial melting” in the Fig. 9.

4. 12 figures in the manuscript are too many for a paper. I suggest deleting or merging some of them. The captions of several important figures are too simple (e.g., Figure 9 and 10). It will be better for understanding if more illustrations are added in

the captions.

Reply: According to the reviewer's suggestion, we have deleted Fig. 6 and Fig. 10 and added detailed description of some important figures.

Reviewer #2:

The paper by Chen et al deals with the formation processes of dunites and chromitites in some Turkish ophiolites via Li isotopes and trace elements in olivine.

The manuscript is well written with only some minor points that should be clarified or added to help the reader.

One of these points is at lines 270-278, where it is written "The chromitites from the two ophiolites display similar Li contents and ^7Li values " and then "the data presented here demonstrate that the composition of trace elements and Li isotopes are different". Maybe, the two sentences need some more explanations. They can't be similar and different at the same time.

Reply: Sorry for this confusion. We meant that compared to different $\delta^7\text{Li}$ compositions of olivine in Orhaneli dunites (3.7 to 11.0‰) and Harmançık dunites (-2.5 to 20.3‰), the $\delta^7\text{Li}$ compositions of olivine in chromitite from the two ophiolites are similar (5.0 to 14.7‰ in Orhaneli and 4.1 to 15.6‰ in Harmançık). This was clarified in the revision.

It is written that there are good correlations between Mn, Ni and Co but Fig. 7c displaying Co vs Mn shows that for some samples Co values are almost constant while Mn changes, while for some other Mn is constant and Co changes. So, I can't see this good correlation.

Reply: There are good correlations between Ni and Mn, whereas the correlation between Co and Mn is un conspicuous. This description has been modified in the revision.

In fig. 12a it is quite difficult to see the boninitic field. Kamenetsky et al (2001) defined a limit between BON and IAT at about 0.4 wt. % TiO_2 , while Derbyshire et al (2013 LITHOS) show an overlapping area but in a logarithmic scale it is difficult to see this without some more scale labels.

Reply: According to the figure 10 of Derbyshire et al. (2013), we added the field of boninite in the Fig. 12a, and found our studied samples are plotted in the field of boninite or the nearby IAT field. In the Fig. 12a, we just want to show that the chromite TiO_2 and Al_2O_3 contents plotted directly into the arc field, suggesting the formation of chromite is closely related to the melts from island arc. In the next Fig 12b-c, we further confirmed that the boninite or boninitic melts could be the parental magma of chromite, based on the Cr# of chromite and the calculated composition of melts in equilibrium with chromitite.

In my opinion Fig. 4 is a bit chaotic and difficult to read.

Reply: More detailed descriptions have been added in the captions, so it is clear to read and understand.

In the tables I can't find the values of Mn in ppm but only as wt. %. Did you calculate the ppm values from the wt. % or did you analyzed it by LA-ICP-MS but it was not reported in the tables?

Reply: The values of Mn and Ni in ppm are analyzed by LA-ICP-MS. We have added these values in the Table 3.

There is a diagram with Mg and Fe²⁺ values for both chromites and olivines but these values are not reported in the tables. Could you, please, add the cation per formula unit of the analyzed minerals.

Reply: We have added the Mg/Fe²⁺ ratios of olivine and chromite to the Table 1 and Table 2, respectively. The MgO and FeO contents of olivine and chromite have been in the Table 1 and Table 2. There is no need to add the Mg and Fe²⁺ values in the tables because the cation Mg and Fe²⁺ is calculated by the MgO and FeO contents of minerals.

Fig. 6 shows Zn vs Co (6a) and Sc vs. Co (6b) of olivine in the dunites and chromitites but in Fig. 6a the scale is 60-160 for Co while it is 250-550 in fig. 6b. I can't understand how it is possible that the range of cobalt is different in the two diagrams. And, however, I'm unable to find a trace element ranging between 250 and 550.

Reply: Sorry for the confusion. The Co contents in the Fig. 6a are the olivine Co contents, while the Co contents in the Fig. 6b are the Co contents of chromite. The Fig. 6 has been deleted in the revision.

Once, Prof Rollinson, author of the book "Using geochemical data", told me that in describing diagram you should say Y vs X so it is MnO vs Fo (Fig. 1) and the same for all the other figures.

Reply: We have modified it in all figure captions.

Other minor points

Line 263: it is written "from 4 to 11" but it seems that the lowest value is 3.7 (OL1 core 5m dunite)

Reply: We modified it.

Line 320: it is written olivine

Reply: We corrected it.

References

Line 56: it is written Pakunc instead of Paktunc

Reply: We corrected it.

Line 713: it should be Jeffcoate with double f

Reply: We modified it.

In the text there are some references that are not present in the reference list such as Zhang et al 2018, Akbulut 2018, Bonavia et al 1993, Ballhaus et al 1991 and Tomascak et al 2000. There is Abily et al 2013 that maybe corresponds to Abily and Ceuleneer 2013, and Tang et al 2009 that could be Tang et al 2011.

The following are written in the reference list but are not cited in the text: Arai and Yurimoto 1994, Coogan et al 2005b, Dick and Bullen 1984, Keleman et al 1992, Richter et al 2014, Su et al 2017, Uysal et al 2009, Xiao et al 2017.

In the text there are two papers by Rospabè et al, one is 2018, the other 2019. In the reference list both are 2018. Check.

Reply: We have checked the references in the text and the references in the reference list, deleted the references which are not cited, added the references which are not present in the reference list but in the text, and confirmed that the references in the text and reference list are same.

Trace elements and Li isotopic compositions of olivine from the mantle-crust transition zone of the Bursa ophiolites (including Orhaneli ophiolite and Harmancık ophiolite) in NW Turkey were measured to constrain the genesis of these dunites and chromitites. A cumulate origin for dunite can be ruled out due to the depletion of incompatible trace elements (Zr, Ti, and heavy rare earth elements) in olivine, instead the chemical signatures point to a replacive origin via melt-rock interaction. The olivine grains in the dunites have lower MnO (0.06-0.15 wt.%), Co (106-137 ppm), Ca (73-323 ppm), and higher NiO (0.23-0.44 wt.%) concentrations than olivine phenocrysts in MORB, suggesting these transition-zone dunites have equilibrated with extremely depleted melts. Additionally, the relatively small $\delta^7\text{Li}$ variations of olivine (average $\delta^7\text{Li}$ +4.8 to +8.7‰) of the Orhaneli suite indicate the Li isotopic compositions of melts percolating through these dunites are relatively homogeneous. However, the large $\delta^7\text{Li}$ variations of olivine (-2.5 to 20.3‰) in Harmancık dunites can be explained by incomplete diffusive equilibration with melts percolating through these dunites, suggesting infiltration happened not long before obduction of the ophiolite. Olivine in chromitites has higher Fo (92.6-94.7) than coexisting dunites, likely induced by subsolidus Mg-Fe exchange between olivine and chromite. The higher chromite contents of the chromitites can also explain the lower concentrations of Sc, V, Co and Zn in coexisting olivine grains. Mixing of depleted mantle-derived melts and boninitic magmas is suggested to induce a compositional shift from the olivine-chromite cotectic line to the liquidus field of chromite, causing the precipitation of chromite and formation of chromitite layers in the dunites. The heavy Li isotopic compositions (+5 to +11‰) of olivine in chromitites and dunites compared to MORB, together with the estimated compositions of parental magmas (Al_2O_3 : 9.8-11.4 wt.%; TiO_2 : 0.22-0.38 wt.%) for the chromitites, indicate an arc-like geochemical affinity, hence a subduction-related setting in which these mantle-crust transition zones formed.

(1) $\delta^7\text{Li}$ study of Orhaneli-Harmancık mantle-crust transition zone dunite and chromitite

(2) Orhaneli dunite formed by interaction of peridotite with homogeneous melt batches

(3) Harmancık dunite reflects incomplete diffusive equilibration during melt percolation

(4) Parental magmas of the chromitites show boninitic geochemical affinities.

1 **Formation processes of dunites and chromitites in Orhaneli and Harmancık**
2 **ophiolites (NW Turkey): evidence from in-situ Li isotopes and trace elements in**
3 **olivine**

4

5 Chen Chen^{1,2,3*}, Jan C.M. De Hoog^{4*}, Ben-Xun Su^{1,3,5}, Jing Wang^{1,3,5}, İbrahim Uysal⁶,
6 Yan Xiao^{3,7}

7

8 ¹ Key Laboratory of Mineral Resources, Institute of Geology and Geophysics, Chinese Academy
9 of Sciences, Beijing 100029, China

10 ² Key Laboratory of Mineralogy and Metallogeny, Guangzhou Institute of Geochemistry, Chinese
11 Academy of Sciences, Guangzhou 510460, China

12 ³ Innovation Academy for Earth Science, Chinese Academy of Sciences, Beijing 100029, China

13 ⁴ Grant Institute, School of GeoSciences, The University of Edinburgh, Edinburgh, EH9 3FE,
14 United Kingdom

15 ⁵ University of Chinese Academy of Science, Beijing, 100049, China

16 ⁶ Department of Geological Engineering, Karadeniz Technical University, 61080 Trabzon, Turkey

17 ⁷ State Key Laboratory of Lithospheric Evolution, Institute of Geology and Geophysics, Chinese
18 Academy of Science, Beijing 100029, China

19

20 *Corresponding authors: chenchen2@gig.ac.cn (Chen Chen)

21 ceesjan.dehoog@ed.ac.uk (Jan C.M. De Hoog)

22

23 **Abstract**

24 Trace elements and Li isotopic compositions of olivine from the mantle-crust
25 transition zone of the Bursa ophiolites (including Orhaneli ophiolite and Harmancık
26 ophiolite) in NW Turkey were measured to constrain the genesis of these dunites and
27 chromitites. A cumulate origin for dunite can be ruled out due to the depletion of
28 incompatible trace elements (Zr, Ti, and heavy rare earth elements) in olivine, instead
29 the chemical signatures point to a replacive origin via melt-rock interaction. The
30 olivine grains in the dunites have lower MnO (0.06-0.15 wt.%), Co (106-137 ppm),
31 and higher NiO (0.23-0.44 wt.%) concentrations than olivine phenocrysts in MORB,
32 suggesting these transition-zone dunites have equilibrated with extremely depleted
33 melts. Additionally, the relatively small $\delta^7\text{Li}$ variations of olivine (average $\delta^7\text{Li}$ +4.8
34 to +8.7‰) of the Orhaneli suite indicate the Li isotopic compositions of melts
35 percolating through these dunites are relatively homogeneous. However, the large
36 $\delta^7\text{Li}$ variations of olivine (-2.5 to 20.3‰) in Harmancık dunites can be explained by
37 incomplete diffusive equilibration with melts percolating through these dunites,
38 suggesting infiltration happened not long before obduction of the ophiolite. Olivine in
39 chromitites has higher Fo (92.6-94.7) than coexisting dunites, likely induced by
40 subsolidus Mg-Fe exchange between olivine and chromite. The higher chromite
41 contents of the chromitites can also explain the lower concentrations of Sc, V, Co and
42 Zn in coexisting olivine grains. Mixing of depleted mantle-derived melts and boninitic
43 magmas is suggested to induce a compositional shift from the olivine-chromite
44 cotectic line to the liquidus field of chromite, causing the precipitation of chromite

45 and formation of chromitite layers in the dunites. The heavy Li isotopic compositions
46 (+6 to +11‰) of olivine in chromitites compared to MORB, together with the
47 estimated compositions of parental magmas (Al_2O_3 : 9.8-11.4 wt.%; TiO_2 : 0.22-0.38
48 wt.%) for the chromitites, indicate an arc-like geochemical affinity, hence a
49 subduction-related setting in which these mantle-crust transition zones formed.

50 **Key words:** olivine; trace element; Li isotopes; ophiolite; chromitite; mantle-crust
51 transition zone

52

53 **1. Introduction**

54 The mantle-crust transition zone is well documented in many ophiolites, and
55 marks the petrological transition from mantle peridotites to lower crustal cumulates
56 (e.g., [Zhang et al., 2017](#); [Rollinson, et al., 2018](#); [Rospabé et al., 2018](#)). Ophiolitic
57 mantle-crust transition zones typically consist of dunite-dominated ultramafic rocks
58 and stratiform-like chromitites, and can reach a thickness of several kilometers
59 ([Paktunc, 1990](#)). These dunites are made of mostly olivine with minor chromite and
60 their thickness ranges from a few meters to a few hundred meters (e.g., [Zhang et al.,](#)
61 [2017](#)). Although the transition zone chromitites are distinguished by their layered
62 morphology from the mantle podiform chromitites which occur as irregular lenses and
63 pods, their compositions are similar in many cases (e.g., [Arai et al., 2004](#); [Rollinson,](#)
64 [2008](#)). Despite many years of investigation, the genesis of the dunites and chromitites
65 in the ophiolitic mantle-crust transition zone is still debated, and different models
66 have been proposed, such as magmatic cumulates stagnating at the base of the crust

67 (e.g., [Abily and Ceuleneer, 2013](#)), crustal assimilation ([Arai et al., 2004](#)), reactions
68 between melts and mantle harzburgites (e.g., [Abily and Ceuleneer, 2013](#)), and mixing
69 of mantle-derived melts with differentiated magmas (e.g., [Ballhaus, 1998](#)). In addition,
70 the nature of the mixed or infiltrated melts and their influences on the mantle-crust
71 transition zone are not yet well known, limiting our understanding of the evolution of
72 ophiolites. A close link between subduction initiation and chromitite/ophiolite genesis
73 has been documented (e.g., [Reagan et al., 2017](#); [Zhang et al., 2017](#)) in several studies
74 of the extensive ophiolites in Turkey (e.g., [Uysal et al., 2017](#); [Chen et al., 2019](#)).
75 Therefore, careful study of the formation processes of the chromitite and their tectonic
76 setting could shine further light on the relationship between subduction initiation and
77 ophiolite emplacement.

78 Olivine is a ubiquitous mineral in both the ultramafic and mafic igneous rocks,
79 and in most cases, it is the first silicate phase to crystallize from ultramafic-mafic
80 melts ([Foley et al., 2013](#)). Olivine thus controls early magmatic differentiation
81 processes, but its Fo content can provide little information about its origin and
82 evolution ([De Hoog et al., 2010](#); [Foley et al., 2013](#)), which forces us to focus on its
83 trace element geochemistry. Consequently, it has become increasingly important to
84 improve our knowledge of the trace element composition of olivine, and to test the
85 use of its geochemical signature as a tracer of early igneous and mantle melting
86 processes ([Foley et al., 2013](#); [Rampone et al., 2016](#)). Several studies have shown that
87 olivines in peridotites from different tectonic environments and/or various origins
88 exhibit distinct geochemical characteristics and define systematic elemental

89 correlations for a series of trace elements (Ni, Mn, Zn, Co, Zr and heavy rare earth
90 elements (HREE)), recording different magmatic processes (Sobolev et al., 2007; De
91 Hoog et al., 2010; Foley et al., 2013; Rampone et al., 2016). Recent work on the
92 Purang and Luobusa ophiolites (Su et al., 2019) advocates that the incompatible trace
93 elements of olivine are more sensitive to melting processes, whereas the
94 concentrations of compatible trace elements are mostly constrained by their source
95 composition.

96 Lithium and its isotopes (^6Li and ^7Li) are increasingly used to trace multiple
97 high-temperature processes due to their moderate incompatibility, strong fluid
98 mobility, and large mass difference (17%) between its two isotopes (e.g., Tomascak et
99 al., 2016). Olivine is the dominant Li reservoir in the upper mantle (Seitz and
100 Woodland, 2000; De Hoog et al., 2010), and olivine-melt partition coefficients of Li
101 are virtually independent of pressure, temperature and olivine composition (Seitz and
102 Woodland, 2000; Qian et al., 2010). The equilibrium fractionation of Li isotopes is
103 likely to be negligible at high temperatures (Vlastelic et al., 2009). However, many
104 natural peridotites display heterogeneous $\delta^7\text{Li}$ compositions, which has been
105 attributed to Li diffusion or interaction between percolating melts and peridotites (e.g.,
106 Lundstrom et al., 2005; Rudnick and Ionov, 2007; Su et al., 2014). Thus, olivine Li
107 isotopic systematics can be used to trace magmatic processes of mantle-crust
108 transition zone dunites and chromitites.

109 In the Bursa ophiolites (Orhaneli and Harmancik ophiolites) in northwestern
110 Turkey, mantle-crust transition zones typically contain interlayered dunites and

111 chromitites (Uysal et al., 2015), the successions of which can reach up a few
112 kilometers thick. In this paper, we provide in-situ trace element and Li isotope
113 analyses of olivine in the chromitites and dunites from the mantle-crust transition
114 zones of Orhaneli and Harmancık ophiolites. These datasets, together with
115 petrological investigations and mineral major oxide compositions, are used to
116 constrain the magmatic processes involved in the formation of dunites and chromitites
117 in ophiolitic mantle-crust transition zones.

118

119 **2. Geological Setting**

120 Tethyan ophiolites in Anatolia occur in several E-W trending belts, which are
121 separated by a series of Gondwana-derived continental fragments (e.g., Uysal et al.,
122 2014) (Fig. 1a). The Izmir-Ankara Suture Zone (IASZ) in northern Turkey occurs
123 between the Sakarya Zone (continent) to the north and the Anatolide-Tauride
124 continental block to the south (Fig. 1a), and has relatively intact ophiolite blocks,
125 which are locally extensive and well preserved (Dilek and Thy, 2006). The Orhaneli
126 and the Harmancık ophiolites, situated in the western part of the IASZ, are considered
127 as remnants of the Izmir-Ankara-Erzincan ocean, a local term for the northern branch
128 of the Neotethys ocean (Sarifakioğlu et al., 2009). The Orhaneli ophiolite was
129 tectonically emplaced onto northwestern Anatolia along the IASZ (Fig. 1a). The
130 Harmancık ophiolite is located ca. 30 km south of the Orhaneli ophiolite (Fig. 1b)
131 (Sarifakioğlu et al., 2009). These two ophiolites were thrust southwards over the
132 metamorphic basement rocks of the Tavşanlı zone in the Anatolide-Tauride platform

133 (Sarifakioğlu et al., 2017).

134 The Orhaneli ophiolite is approximately 50 km long, 15 km wide and 1500 m
135 thick (Fig. 1b; Sarifakioğlu et al., 2009), and mainly consists of mantle-crust
136 transition zone comprising mostly basal ultramafic cumulates. The transition zone is
137 dominated by chromitite interlayered dunites, followed by wehrlites, lherzolites,
138 harzburgites and pyroxenites and to a lesser extent mafic cumulates such as gabbros
139 and gabbronorites (e.g., Sarifakioğlu et al., 2009; Uysal et al., 2015). The chromitites
140 interlayer with dunite in the two ophiolites and have typically semi-massive and
141 banded (stratiform, cumulate) structures (Fig. 2). The mantle-crust transition zone of
142 the Harmancık ophiolite, which reaches up to 1000 m thickness, has similar rock
143 assemblages to those of the Orhaneli ophiolite (Tankut, 1980). The Harmancık
144 ophiolite contains additional podiform chromitites in its mantle section (Sarifakioğlu
145 et al., 2009). The podiform chromitites form centimeters to meters scale
146 lenticular/tabular orebodies enclosed in thick dunite envelopes within mantle
147 harzburgites. The mantle harzburgites and dunites from Harmancık ophiolite have
148 been almost completely altered to serpentine and talc, and are unconformably overlain
149 by Neogene sedimentary units (e.g., Uysal et al., 2014, 2015).

150

151 **3. Petrography of dunites and chromitites**

152 In the Orhaneli ophiolite, dunites display adcumulate textures and consist of
153 mostly medium- to fine-grained olivine crystals with minor chromites (Fig. 3a, b).
154 Chromitites generally show adcumulus- to orthocumulus-like textures with euhedral

155 to subhedral chromite grains (Fig. 3c). They occur as bands and layers in dunites (Fig.
156 2a-c), and massive chromitites are very rare. The banded chromitite orebodies display
157 schlieren textures, characterized by parallel layers of chromitite alternating with
158 dunite (Fig. 2b). The thickness of the chromitite bands in the Orhaneli ophiolite
159 typically ranges between 0.2 and 3 cm, rarely reaching up to 5 cm (Fig. 2b-c). In
160 contrast, chromitites from the Harmancık mantle-crust transition zone occur as
161 schlieren/bands, semi-massive, and disseminated textures. Chromite grains are mostly
162 euhedral to subhedral. Dunites are made up predominantly of olivine (> 95%) and
163 have a dominant cataclastic texture (Fig. 3d).

164 In the Orhaneli ophiolite, the mantle-crust transition zone is nearly horizontal
165 (Fig. 2a), and we have selected 13 samples (dunites and chromitites) from the
166 mantle-crust transition zone profile. The thickness of this profile is about 90 m and we
167 fixed the base of the dunite as 0 m and its roof is +90 m. In the Harmancık ophiolite,
168 12 drill hole samples from the mantle-crust transition zone were selected for chemical
169 analyses, owing to their pristine olivine grains. The drill hole samples including
170 dunite and chromitite were collected from depths of 63.4 m to 73.4 m.

171

172 **4. Analytical methods**

173 **4.1 Major oxide analysis of minerals**

174 Major oxide compositions of olivine and chromite were determined by
175 wavelength-dispersive X-ray spectrometry using a JEOL JXA8100 electron probe
176 micro-analyzer at the Institute of Geology and Geophysics, Chinese Academy of

177 Sciences (IGGCAS). The analyses were carried out using an accelerating voltage of
178 15 kV, a 10 nA beam current, a 5 μm spot size and 10-30 s peak counting time.
179 Natural and synthetic mineral standards were used for calibration. A ZAF procedure
180 was used for matrix corrections. Typical analytical uncertainty for the analyzed
181 elements was better than 1.5% (1RSD%).

182 **4.2 Trace element analysis of olivine**

183 In-situ trace element analyses of olivine were conducted on thin sections using a
184 laser ablation inductively coupled plasma mass spectrometer (LA-ICP-MS) at
185 IGGCAS. The LA-ICP-MS system consists of a 193 nm Coherent COMPex Pro ArF
186 Excimer laser coupled to an Agilent 7500a ICP-MS. About 6-8 spots were measured
187 for different olivine grains in each sample. The laser spot size was 140 μm , and the
188 repetition rate was 8 Hz. Each analysis consisted of 60 s measurement of gas blank
189 and 60 s ablation. The following isotopes were measured: ^7Li , ^{27}Al , ^{29}Si , ^{31}P , ^{39}K , ^{43}Ca ,
190 ^{45}Sc , ^{49}Ti , ^{51}V , ^{53}Cr , ^{59}Co , ^{66}Zn , ^{91}Zr , ^{163}Dy , ^{166}Er , ^{172}Yb . [De Hoog et al. \(2010\)](#)
191 reported that potential interferences in olivine from matrix components MgO , SiO_2
192 and FeO , which are generated during ablation only and therefore unaccounted for by
193 gas blank subtraction. The contribution of $^{26}\text{Mg}^{40}\text{Ar}$ to the ^{66}Zn signal is about 0.2
194 ppm, and the $^{29}\text{Si}^{16}\text{O}$ interference on ^{45}Sc accounted for 0.2 ppm of the signal ([De](#)
195 [Hoog et al., 2010](#)), hence those are small enough to be ignored. A glass standard,
196 NIST 610, was used for external calibration. For most of the trace elements NIST 612
197 standard was used to monitor instrument drift, and silicon (^{29}Si) was selected as an
198 internal standard. The SiO_2 contents of NIST 610 and NIST 612 are 69.7% and 72.1%,

199 respectively. Reference values of NIST 610 and NIST 612 are from GeoREM
200 (<http://georem.mpch-mainz.gwdg.de>). The data were reduced using the GLITTER 4.0
201 program.

202 **4.3 Li concentration and isotope analyses of olivine**

203 In-situ analyses of Li concentrations and isotopic ratios of olivine were carried
204 out on gold-coated polished thin-sections using a Cameca IMS 1270 SIMS at the
205 Edinburgh Ion Microprobe Facility, in the University of Edinburgh, United Kingdom.
206 A $^{16}\text{O}_2$ primary ion beam with an intensity of 12-16 nA was accelerated to 22.5 kV
207 and impacted onto the sample surface using Kohler illumination. The elliptical spot
208 area was approximately $20 \times 30 \mu\text{m}$. The secondary ion beam position in the field
209 aperture and the ^7Li peak position were automatically centered before each
210 measurement during a 60-s pre-sputter without beam rastering. Secondary ions were
211 counted in mono-collection, pulse-counting mode. Fifty cycles were measured with
212 counting times of 6 and 2.5 s for ^6Li and ^7Li , respectively. The count rate for ^7Li
213 ranged from 30,000 to 120,000 cps, depending on the Li concentration of the sample
214 and primary beam intensity, resulting in 1 s uncertainties of $\delta^7\text{Li}$ of 0.5-1.2‰.
215 Lithium concentrations were calculated using beam current corrected ^7Li count rates
216 of samples using 06JY34O1 as a standard (Li concentration = 1.73 ppm; [Su et al.,](#)
217 [2015](#)). The Li isotopic ratios are expressed as $\delta^7\text{Li}$ relative to the NIST L-SVEC
218 standard $\{\delta^7\text{Li} = [({}^7\text{Li}/{}^6\text{Li})_{\text{sample}}/({}^7\text{Li}/{}^6\text{Li})_{\text{L-SVEC}} - 1] \times 1000\}$. Basaltic standards
219 BCR2-G and ML3B-G were analyzed to monitor instrument drift, whereas 06JY34O1
220 ($\delta^7\text{Li} = 3.1\text{‰}$; [Su et al., 2015](#)) was used for calibration. Matrix composition (Fo

221 content) has an effect on measured olivine Li isotopic compositions; e.g., [Su et al.](#)
222 (2015) showed that $\delta^7\text{Li}$ values increase by 1.0‰ for each mole percent decrease in
223 the Fo content of olivine, and this was taken into account for calibration. As Fo
224 contents of the olivines span a narrow range from 91.6 to 94.7, the matrix correction
225 amounted to no more than 3‰, compared to a range of > 20‰ in $\delta^7\text{Li}$ for the whole
226 dataset.

227

228 **5. Results**

229 **5.1 Major oxide contents of minerals**

230 Olivine in the Orhaneli and Harmancık dunites has Fo values of 92.4-94.0 and
231 91.6-93.5, respectively ([Table S1](#); [Fig. 4a-c](#)). The chromitites contain olivine with
232 somewhat higher Fo values (92.6-94.7 in Orhaneli; 93.3-94.4 in Harmancık) than
233 those in the dunites ([Table S1](#)). The dunites from the two ophiolites have similar MnO
234 (0.06-0.15 wt.%) and NiO (0.23-0.44 wt.%) contents in their olivine ([Table S1](#)). In the
235 Orhaneli and Harmancık profile analyses, the variations of Mn concentrations in
236 olivines are not continuous and yield abrupt change at the contact with chromitite
237 layers. Compared to Mn, Ni concentrations show the reverse patterns ([Fig. 5](#)).

238 Chromite grains in dunites of the both ophiolites are generally uniform in TiO_2
239 contents (0.14-0.23 wt.% in Orhaneli; 0.11-0.22 wt.% in Harmancık), similar to those
240 in the chromitites (0.14-0.26 wt.% and 0.13-0.22 wt.%), whereas their Cr# ($100 \times$
241 $\text{Cr}/(\text{Cr}+\text{Al})$) and Mg# ($100 \times \text{Mg}/(\text{Mg}+\text{Fe})$) values are variable within ranges of
242 79.1-81.8 and 47.6-53.5 in the Orhaneli dunites, 70.6-80.2 and 41.9-52.9 in the

243 Harmancık dunites, 81.1-82.8 and 58.7-67.3 in the Orhaneli chromitites and 78.8-80.0
244 and 46.4-64.2 in the Harmancık chromitites (Table S2; Fig. 4).

245 **5.2 Trace element compositions of olivine**

246 From base to top, the mantle-crust transition zone in the Orhaneli ophiolite
247 includes many cyclic dunite and chromitite layers (Fig. 2a-b) with a total thickness of
248 90 m. Overall, olivines in chromitites show lower Co, Zn, Sc and V concentrations
249 than those in dunites (Fig. 5a, b). The Co concentrations of olivine in the dunites
250 (106-132 ppm in Orhaneli, 128-137 ppm in Harmancık) are higher than those of
251 primitive mantle (105 ppm; McDonough and Sun, 1995), whereas the concentrations
252 of Zn (6.0-44.8 ppm), Sc (2.14-3.68 ppm) and V (0.07-0.36 ppm) in all samples are
253 lower than primitive mantle (Zn: 55 ppm; Sc: 16.2 ppm; V: 82 ppm; McDonough and
254 Sun, 1995). The olivine in both dunites and chromitites from the two ophiolites has
255 lower incompatible trace element concentrations (Ti = 4.0-7.8 ppm, Zr = 0.010-0.034
256 ppm, and Yb = 0.007-0.027 ppm) than the counterparts in olivine phenocrysts in
257 MORB (Table S3; Fig. 6) (e.g., Piccardo et al., 2007; Foley et al., 2011). In the
258 Orhaneli section and Harmancık drill hole samples, there is no apparent correlation
259 between trace element compositions of olivine and the relative position of the layers
260 (Figs. 5, 6).

261 **5.3 Li concentrations and isotopic compositions**

262 In the Orhaneli dunites, olivine has Li concentrations varying from 0.9 to 1.5
263 ppm, and $\delta^7\text{Li}$ from 3.7 to 11.0‰ (Fig. 7), with no correlation between Li
264 concentrations and Li isotopic compositions (Fig. 8). In contrast, Li concentrations

265 (0.7 to 1.9 ppm) and $\delta^7\text{Li}$ values (-2.5 to 20.3‰) of olivine in the Harmancık dunites
266 vary widely (Table S1), and the $\delta^7\text{Li}$ values are negatively correlated with the Li
267 concentrations (Fig. 8). Most olivine grains in the two ophiolites show little change in
268 Li concentrations and $\delta^7\text{Li}$ values from core to rim (Table S1). Nevertheless, different
269 olivine grains in the same sample from Harmancık can have strongly variable Li
270 isotopic compositions (up to 15‰ difference) (Table S1; Fig. 7). On the other hand,
271 the chromitites from the two ophiolites display Li contents and $\delta^7\text{Li}$ values of olivine
272 with 0.8 to 1.6 ppm and 5.0 to 14.7‰ in Orhaneli and 0.7 to 1.2 ppm and 4.1 to 15.6‰
273 in Harmancık (Table S1; Fig. 7).

274

275 **6. Discussion**

276 Based on trace elements and Li isotopes compositions of olivine in the dunites
277 and chromitites from the mantle-crust transition zones for both ophiolites, we first
278 evaluate the various processes that may account for the observed trace elemental and
279 Li isotope variations, followed by models for the formation of dunites and
280 chromitites.

281 **6.1 Origin of mantle-crust transition zone dunites in the Orhaneli and** 282 **Harmancık ophiolites**

283 Dunite consists almost entirely of olivine and is usually formed by one of three
284 processes (e.g., Su et al., 2016; Yao et al., 2018): 1) ultrahigh-degree partial melting of
285 mantle with nearly all orthopyroxene being exhausted; 2) cumulate dunite left behind
286 by the fractionation and accumulation of abundant olivine from an ultramafic-mafic

287 magma; 3) reaction between silica-undersaturated melt migrating in channels and
288 pyroxene-rich wall rock triggering the formation of replacive dunite.

289 Cumulate dunites are formed via crystal accumulation from magmas and
290 therefore olivine generally has low Fo (88-91) and feature a rapid decrease in the NiO
291 content with decreasing Fo (Santos et al., 2002; Song et al., 2007; Arai et al., 2012;
292 Seo et al., 2013; Su et al., 2016; Rospabé et al., 2018). Moreover, the coexisting
293 chromites show a wide range of Cr# from 15 to 76 as well as high TiO₂ contents (up
294 to 0.8 wt.%) (Santos et al., 2002; Song et al., 2007; Arai et al., 2012; Seo et al., 2013)
295 (Fig. 4a-c). In contrast, olivine in replacive dunites generally has higher Fo values (up
296 to 94), because the high-MgO melts reacting with peridotites convert olivine and
297 pyroxene in peridotite to high-Fo olivine (Rollinson et al., 2018). Besides, no obvious
298 correlation exists between the Fo and NiO of olivine grains within the replacive
299 dunites (Mazzucchelli et al., 2009). In the Orhaneli and Harmancık dunites, olivine
300 has higher Fo (91.6-94.0) and lower MnO contents (0.06-0.15 wt.%) than that from
301 cumulate dunites, while chromites display higher Cr# (79.1-82.8) and lower TiO₂
302 contents (0.14-0.26 wt.%) (Fig. 4c-d). These observations, together with the absence
303 of a clear correlation between Fo and NiO in olivine, demonstrate that the dunites
304 from both ophiolites could not be related to fractional crystallization (Fig. 4b). Instead,
305 all our data fall within the fields of replacive dunites (Fo: 90.4-94.6; MnO of olivine:
306 0.07-0.15 wt.%; Cr# of chromite: 23-89) (Suhr et al., 2003; Piccardo et al., 2007;
307 Ackerman et al., 2009; Mazzucchelli et al., 2009; Oh et al., 2012; Sanfilippo et al.,
308 2014, 2017) (Fig. 4), indicating that these dunites were formed by melt-peridotite

309 interaction rather than have a cumulate origin. Furthermore, although the olivines
310 from these dunites show a good correlation between Ni and Mn, the correlation
311 between Co and Mn is poor (Fig. 6b-c). According to olivine-melt partition
312 coefficients (e.g., Beattie et al., 1991), Co and Ni are compatible in olivine, whereas
313 Mn is incompatible, and hence segregation of olivine from its parental magma should
314 produce a decrease of Co and Ni with increasing Mn (Sanfilippo et al., 2014).
315 However, Co contents in olivine from the Orhaneli and Harmancık dunites are poorly
316 correlated with Mn contents, and therefore incompatible with olivine fractionation
317 and likely to be induced by melt migration.

318 For the Orhaneli and Harmancık ophiolites, the mineralogical and geochemical
319 characteristics of mantle-crust transition zone dunites indicate that they were formed
320 by melt-peridotite interaction: orthopyroxene + melt 1 \rightarrow olivine + melt 2. In this
321 reaction, melt 1 (reactant) is silica-undersaturated and melt 2 (product) is relatively
322 enriched in SiO₂ and Cr₂O₃ due to progressive melt-rock reaction (e.g., Suhr, 1999;
323 Zhou et al., 2005). Since the majority of all dunites are of refractory chemical nature
324 and not akin to MORB (Figs. 4, 6), we argue that the reactant (melt 1) was highly
325 depleted.

326

327 **6.2 Origin of chromitites of the Orhaneli and Harmancık ophiolites**

328 Olivines in Orhaneli and Harmancık chromitites have somewhat higher Fo than
329 that contained in dunites, which likely implies an additional process for the
330 chromitites. Subsolidus Mg-Fe exchange between olivine and chromite has been

331 usually reported in chromitites (e.g., [Xiao et al., 2016](#)):



333 The Mg diffuses from chromite to olivine and Fe from olivine to chromite. The
334 compositional effect of Fe-Mg exchange on olivine depends on the elemental contents
335 and relative modal abundances of olivine and chromite in the rocks ([Xiao et al., 2016](#)).
336 The Fe-Mg exchange effect on olivine in the dunites is negligible because of the
337 extremely low amount of chromite. Recent studies (e.g., [Qian et al., 2010](#)) reported
338 that despite differences in ionic size and charge, Sc and V diffuse at approximately
339 similar rates to Mg, Fe and other divalent cations (e.g., Co and Zn). Cobalt and Zn are
340 more compatible in chromite than in olivine, with crystal-melt partition coefficients
341 from 8.3 to 2.1, and 7.9 to 3.6, respectively (<https://earthref.org>). Vanadium
342 compatibility decreases in the order of chromite >> pyroxene >> olivine
343 ([Witt-Eickschen and O'Neill et al., 2005](#)). In addition, the partitioning of Sc between
344 chromite and olivine is strongly dependent upon the major element composition of
345 chromite ([Stosch et al., 1981](#)). Thus, as expected, Co, Zn, Sc and V concentrations of
346 olivine in the Orhaneli profile and Harmancık chromitites are lower than those in the
347 associated dunites ([Figs. 5a-b](#)), which points to the relative modal abundances of
348 chromite and olivine being a factor in determining the Sc, V, Co and Zn
349 concentrations in olivine in chromitites ([Xiao et al., 2016](#); [Zhang et al., 2017](#)). For
350 example, in the Orhaneli profile, chromitite sample (+50 m) contains the highest
351 modal amount of chromite and its olivine has the lowest Co, Zn, Sc and V
352 concentrations ([Fig. 5a](#)).

353 Mantle-derived magmas generally have ca. 500 ppm Cr concentrations, whereas
354 the chromites derived from these melts contain 30-50 wt.% Cr₂O₃ (Zhou et al., 2014;
355 Zhang et al., 2017). During the evolution of magmatic systems, the oversaturation of
356 chromite in the magma is an important factor for the formation of chromitite. Addition
357 of silica to magmas has been widely accepted as a means of triggering chromite
358 precipitation, because SiO₂ addition can decrease Cr solubility (Irvine et al., 1986).
359 The increase in silica has been usually attributed to assimilation/reaction of more
360 siliceous materials or magma mixing (e.g., Arai et al., 2004; Zhou et al., 1994, 2014;
361 Zhang et al., 2017). In this regard, chromitites in the Orhaneli and Harmancık
362 mantle-crust transition zones are exclusively associated with dunites, and hence it is
363 unlikely that the oversaturation of chromite was caused by extensive assimilation of
364 siliceous-rich crust. Instead, the oversaturation of chromite induced by magma mixing
365 becomes the most likely scenario here. Mantle-derived mafic magma A rises through
366 the upper mantle and mixes with more Si-rich and Cr-rich magma (e.g., Lissenberg
367 and Dick, 2008), upon which the newly-formed, mixed magma B would move into
368 the field of chromite crystallization (Fig. 9). Additionally, the residual melt (melt 2)
369 following melt-peridotite reaction and orthopyroxene dissolution will also be enriched
370 with Cr and SiO₂ relative to the infiltrating melt (Arai and Yurimoto, 1995).
371 Therefore, it would further facilitate the oversaturation of chromite in the mixed
372 magma (Zhou et al., 1994, 2014; Su et al., 2019), driving crystallization of abundant
373 chromite and forming chromitite layers. Due to precipitation of chromite, mixed
374 magma 'B' would evolve to point 'C', i.e., back to the chromite-olivine cotectic line.

375

376 **6.3 Origin of infiltrating melts**

377 During melt-peridotite interaction, trace elements between minerals and melts
378 can be redistributed. The trace elements of olivine in the Orhaneli and Harmancık
379 dunites do not show any zoning (Tables S1, S3), indicating that they were fully
380 equilibrated with the percolating melts. Since dunites predominantly consist of olivine
381 grains, and other silicate minerals (e.g., pyroxene) are rare or absent, the trace element
382 concentrations of olivine cannot be affected by subsolidus re-equilibration among
383 silicate minerals. Thus, the olivine trace elements can be used to trace the composition
384 of the melt in chemical equilibrium with these crystals. The lower incompatible trace
385 element concentrations (Zr, Ti and HREE) in olivines from the Orhaneli and
386 Harmancık dunites relative to those of the olivines from the lower crustal sections of
387 ophiolites (Sanfilippo et al., 2014) (Fig. 6a) indicate that our dunites are not in
388 equilibrium with a melt derived from the lower oceanic crust. In addition, compared
389 to mantle harzburgites of the Orhaneli and Harmancık ophiolites (chromite Cr#: 43-55;
390 Fo < 91.6) (Uysal et al., 2017), the mantle-crust transition zone dunites have Cr# in
391 chromite of 79-82, NiO in olivine of 0.2-0.4 wt.% and Fo of 91.6-94.0, which are far
392 more refractory. The Mn and Co abundances of olivines in both the Orhaneli and
393 Harmancık dunites are lower than those of olivine phenocrysts within MORB
394 (Sobolev et al., 2007) (Fig. 6b-c), in conjunction with the lower trace-element
395 concentrations relative to primitive mantle (McDonough and Sun, 1995), suggesting
396 that these dunites were equilibrated with melts that are more depleted than MORB

397 (e.g., [Piccardo et al., 2004](#); [Sanfilippo and Tribuzio, 2011](#)).

398 We can use the composition of the chromitites to put further constraints on the
399 composition of its parental melts. In contrast to the incompatible elements, diffusion
400 of compatible elements Cr, Al and Ti out of chromite is negligible ([Abily and
401 Ceuleneer, 2013](#)), because Al and Ti enter olivine and/or serpentine in only very low
402 amounts (e.g., [Kamenetsky et al., 2001](#)). As a consequence, we can use these elements
403 to calculate the composition of equilibrated melts based on chromite compositions.
404 The TiO₂ content of chromite is a key indicator of tectonic setting of where chromitite
405 forms (e.g., [Kamenetsky et al., 2001](#)). The Orhaneli and Harmancık chromites have
406 very low TiO₂, and plot in the arc or boninitic fields ([Fig. 10a-b](#)), suggesting
407 crystallization from low-Ti island arc tholeiitic melts or boninitic melts. In addition,
408 several studies have also shown that chromite compositions in chromitites reflect the
409 composition of their parental melt ([Kamenetsky et al., 2001](#); [Rollinson, 2008](#); [Zhou et
410 al., 2014](#); [Rollinson and Adetunji, 2015](#); [Chen et al., 2019](#)). The following equations
411 were proposed by [Rollinson and Adetunji \(2015\)](#) to more closely reflect the empirical
412 correlations defined by [Kamenetsky et al. \(2001\)](#) and applies to melt with an arc
413 affinity:

414
$$(\text{Al}_2\text{O}_3)_{\text{melt}} = 5.2181 \times \ln(\text{Al}_2\text{O}_3)_{\text{Chr}} - 1.0505 \text{ (Eq. 2)}$$

415
$$(\text{TiO}_2)_{\text{melt}} = 1.0963 \times (\text{TiO}_2)_{\text{Chr}}^{0.7863} \text{ (Eq. 3)}$$

416 The implementation of equations (2) and (3) demonstrates that the melts in
417 equilibrium with chromitite have the following composition: 9.8-10.8 wt.% Al₂O₃ and
418 0.23-0.38 wt.% TiO₂ in Orhaneli, and 10.7-11.4 wt.% Al₂O₃ and 0.22-0.33 wt.% TiO₂

419 in Harmancık. The inferred parental melts of the chromitites from the two ophiolites
420 have similar Al₂O₃ and TiO₂ contents to boninitic melts (Fig. 10c), suggesting that the
421 Orhaneli and Harmancık chromitites possibly originated in a forearc setting during the
422 early stage of subduction. The zigzag pattern (Fig. 5) of the olivine trace element
423 contents in the chromitites from the Orhaneli profile and Harmancık drill hole, in
424 conjunction with the widespread occurrence of interlayered chromitites and dunites,
425 could be the witness of multiple magma replenishments in the mantle-crust transition
426 zone.

427

428 **6.4 Lithium isotope constraints on the origin of Orhaneli and Harmancık** 429 **dunites and chromitites**

430 Due to the highly depleted composition of dunites and chromitites, traditional
431 chemical indicators of tectonic setting can generally not be applied. However, Li
432 isotope systematics of olivine may provide clues about the tectonic setting of the
433 infiltrating melts. High-temperature partial melting is thought to induce negligible Li
434 isotope fractionation (e.g., Tomascak et al., 1999; Ionov and Seitz, 2008) and
435 Jeffcoate et al. (2007) estimated that the $\delta^7\text{Li}$ value of magmas generated by
436 equilibrium melting would be < 0.5‰ different from their source. In addition, most
437 studies have shown that Li isotopes do not fractionate during fractional crystallization
438 of silicate magmas (e.g., Tomascak et al., 1999; Teng et al., 2006). Many studies also
439 demonstrated that diffusion is an important mechanism controlling Li abundances and
440 isotopic distribution (e.g., Su et al., 2014; Tomascak et al., 2016). Lithium

441 concentrations and isotopes do not show core-to-rim zoning in individual olivine
442 grains in most samples of the Orhaneli and Harmancik ophiolites (Table S2), and
443 chromite contains little or no Li (e.g., Jeffcoate et al., 2007; Chen et al., 2019). Thus,
444 the Li isotopic compositions of olivine have not been affected by inter-mineral
445 diffusion. Therefore, the Li isotopic compositions of olivines in the Orhaneli and
446 Harmancik dunites record the history of melt-rock interaction.

447 Compared to typical mantle peridotites with $\delta^7\text{Li}$ values of 2-6‰ and 1.0-1.8
448 ppm Li (Seitz and Woodland, 2000; Su et al., 2014), the olivines from the Orhaneli
449 dunites show a similar range of Li concentrations (0.9-1.5 ppm), but a slightly larger
450 range of $\delta^7\text{Li}$ values (+4.0 to +11.0‰) (Table S1; Figs. 7, 8), offset to higher values.
451 As the samples are relatively homogeneous (1s 0.8-1.7‰ based on multiple olivine
452 analyses in each sample) (Fig. 7) and the olivines are unzoned, these samples likely
453 reached Li isotope equilibrium during rock-melt interaction, and therefore could
454 reflect the composition of the infiltrating melt. Average $\delta^7\text{Li}$ per sample shows a more
455 restricted range from +4.8 to +8.7‰ with 1.1-1.3 ppm Li, suggesting reaction with
456 relatively homogeneous melt batches.

457 The Orhaneli chromitites have somewhat higher $\delta^7\text{Li}$ values (average $\delta^7\text{Li}$ per
458 sample +6.0 to +10.6‰ with 1.0-1.3 ppm), but the two samples with highest $\delta^7\text{Li}$
459 shows considerable heterogeneity (based on multiple olivine analyses in each sample)
460 of > 4-7‰ even though individual olivines are unzoned. Excluding these samples, the
461 range of Orhaneli chromitites is +6.0 to +8.2‰, an even smaller range than the
462 dunites. These Li isotopic characteristics could be attributed to infiltrating melts in a

463 subduction zone setting. Dehydration of altered oceanic crusts during subduction can
464 induce that the Li isotope fractionation generates isotopically heavy-Li fluids and
465 light-Li slab residues (e.g., [Elliott et al., 2004](#); [Penniston-Dorland et al., 2017](#)), but the
466 Li isotopic range of arc lavas (-1 to +12‰) reflects the heterogeneity of the altered
467 oceanic plate and overlying sediments ([Tomascak et al., 2002](#); [Elliott et al., 2004](#)).
468 Mixing of various slab components and re-equilibration with Li already present in the
469 mantle wedge results in arc lavas with $\delta^7\text{Li}$ values that only slightly extend beyond
470 that of MORB. The dominance of $\delta^7\text{Li}$ values in the Orhaneli mantle-crust transition
471 zone that extends well beyond the MORB/mantle peridotite range point to a
472 ubiquitous subducting slab component present in the infiltrating melts. The survival of
473 these signatures suggests that the source of the interacting agent was rather shallow,
474 as Li isotopic signatures will re-equilibrate with ambient mantle at short length and
475 timescales ([Halama et al., 2009](#)). This is consistent with a subduction initiation.

476 Compared to Orhaneli, olivine from the Harmancık dunites shows much larger
477 $\delta^7\text{Li}$ variations of -2.5‰ up to +20.3‰, but also larger sample heterogeneity, with
478 only one sample having a ranging of $\delta^7\text{Li}$ of < 3‰ ([Figs. 7, 8](#)). The Harmancık
479 dunites were considerably more altered than the Orhaneli dunites, but the olivine
480 grains selected for Li isotope analyses were fresh and unzoned, and hence the
481 influences of alteration (such as serpentinization) on $\delta^7\text{Li}$ values between different
482 grains are likely to be small (e.g., [Lundstrom et al., 2005](#)). The larger range of $\delta^7\text{Li}$
483 values in the Harmancık dunite may indicate the infiltrating melts with a wider range
484 of $\delta^7\text{Li}$ values, especially given that the slab-derived fluids and melts have a broad

485 range of compositions and are highly variable from one location to another (Elliott et
486 al., 2004; Yao et al., 2018). However, the heterogeneous distribution of $\delta^7\text{Li}$ in
487 individual samples from the Harmancık dunites and the negative correlation between
488 $\delta^7\text{Li}$ values and Li concentrations is indicative of incomplete diffusive equilibration
489 between olivines and infiltrating melts (Fig. 8) (e.g., Jeffcoate et al., 2007;
490 Penniston-Dorland et al., 2017), which is consistent with the studies of olivine Li
491 isotope of dunite from Trinity ophiolite (Lundstrom et al., 2005) and Luobusa
492 ophiolite (Su et al., 2016). Many studies have demonstrated that ^6Li diffuses about 2-3%
493 faster than ^7Li through melts and minerals (e.g., Lundstrom et al., 2005; Teng et al.,
494 2006). As Li diffuses from percolating melt into olivine, the $\delta^7\text{Li}$ of olivine will
495 become lower at first, but will then increase to higher values until $\delta^7\text{Li}$ equilibrates
496 with that of the infiltrating melt, due to equilibrium partitioning (Lundstrom et al.,
497 2005). During this process, temperature and time are the fundamental parameters that
498 control the efficiency of the isotopic exchange (Tomascak et al., 2016). We, therefore,
499 estimated the equilibration temperatures of the Harmancık and Orhaneli dunites and
500 chromitites based on the Al (Coogan et al., 2014) and Mg-Fe exchange (Ballhaus et
501 al., 1991) between olivine and chromite (Table 1). The Al-in-olivine thermometry
502 results (Coogan et al., 2014) show that the temperature range for Harmancık dunites
503 (933-979°C) is similar to that of the Orhaneli suite (960-993°C), while Mg-Fe
504 exchange temperatures (Ballhaus et al., 1991) are considerably lower: 714-778°C for
505 Orhaneli dunites and 663-755°C for Harmancık dunites. This suggests no significant
506 difference in temperature between Harmancık and Orhaneli ophiolites, so this cannot

507 explain the heterogeneity of the Harmancık samples. The main another factor of
508 diffusion is time. Richter et al. (2014) found that very large lithium isotopic
509 fractionations persisted after the lithium concentration had become effectively
510 homogenized during diffusion process, suggesting that it still takes longer for the
511 isotopic composition to become uniform compared to the time it takes for diffusion to
512 homogenize the total lithium concentration. Thus, if infiltration of melts into the rocks
513 occurred shortly before obduction and exhumation, Li isotopes would not fully
514 equilibrate, and isotope heterogeneity would be preserved during relatively rapid
515 cooling. Heterogeneities in the Harmancık samples could indicate rapid cooling was
516 essential to preserve the observed isotope heterogeneities.

517 In summary, excluding two heterogeneous samples (Fig. 7), the Li isotope
518 signatures of olivine in dunites and chromitites from the Orhaneli ophiolite are likely
519 primary features inherited from their parental melts, with all olivines falling between
520 $\delta^7\text{Li}$ values of +5‰ and +9‰, which is within the range of arc lavas but isotopically
521 heavier than MORB (Fig. 7) (Chan et al., 2002; Tomascak et al., 2002), suggesting an
522 affinity with arc magmatism. The olivine Li isotopic compositions of Harmancık
523 mantle-crust transition zone chromitites are similar to those from Orhaneli, but still,
524 likely have diffusional heterogeneities due to incomplete equilibration between
525 infiltrating melt and olivine. Nevertheless, their average compositions (+6 to +11‰)
526 does suggest a melt source similar to the one that crystallized Orhaneli chromitites.

527 The estimated Al_2O_3 and TiO_2 contents of the parental magmas of chromitites in
528 the two ophiolites are similar to the signatures of boninitic melts. Given that boninitic

529 magmas have been widely found in preserved fore-arcs related to subduction
530 initiation (e.g., [Reagan et al., 2017](#); [Stern et al., 2012](#)), this suggests that the Orhaneli
531 and Harmancık ophiolites possibly originated in a subduction initiation setting, which
532 gives additional support to studies suggesting that these settings represent an ideal
533 environment for forming ophiolites with economically viable chromitite deposits
534 ([Johnson, 2012](#)).

535

536 **7 Conclusions**

537 This study presents in-situ trace elements and Li isotopic compositions of olivine
538 in dunites and chromitites from the Orhaneli and Harmancık mantle-crust transition
539 zone. The following conclusions can be drawn:

- 540 1. Compared to olivine from cumulate dunites, the olivine in the Orhaneli and
541 Harmancık dunites is distinct by higher Ni, lower Mn concentrations and extreme
542 depletion of incompatible trace elements (Ti, Zr and HREE), which are consistent
543 with the formation of dunites driven by interaction of peridotite with depleted
544 melts.
- 545 2. The relatively uniform Li isotopic compositions (+4 to +11‰) of olivines from
546 Orhaneli dunites indicate these samples reached Li isotope equilibrium, and
547 suggest a reaction driven by relatively homogeneous melt batches with a
548 subduction component, whereas the large $\delta^7\text{Li}$ variations (-2.5 to +20.3‰) in
549 olivine from Harmancık dunites reflect incomplete diffusive equilibration during
550 the melt percolation through these dunites.

- 551 3. The formation of chromitites in the mantle-crust transition zone of the two
552 ophiolites was likely triggered by the magma mixing. The calculated Al_2O_3
553 (9.8-11.4 wt.%) and TiO_2 (0.22-0.38 wt.%) contents of the parental magmas of
554 chromitites demonstrate a boninite-like geochemical affinity, i.e., a subduction
555 initiation setting, which is in good agreement with the Li isotopic compositions of
556 their olivines.
- 557 4. In contrast to the dunites, the higher Fo contents of olivine in the chromitites
558 could be caused by the Mg-Fe exchange between olivine and chromite. The lower
559 Sc, V, Co and Zn concentrations of olivine in the chromitites are controlled by the
560 modal abundances of chromite.

561

562 **Acknowledgements**

563 This paper benefited from constructive and detailed comments of two
564 anonymous reviewers, and efficient editorial handling by Xian-Hua Li. This study
565 was supported by the National Natural Science Foundation of China (Grants
566 91755205 and 41772055), and by a Visiting Student grant to Chen Chen from the
567 United Kingdom National Environment Research Council 'Deep Volatiles' program
568 (Grant NE/M000427/1). We thank Wei Lin, Yang Chu and Jie-Jun Jing for the
569 assistance in the field trips in the Kızıldağ.

570 **References**

571 Abily, B., Ceuleneer, G., 2013. The dunitic mantle-crust transition zone in the Oman
572 ophiolite: residue of melt-rock interaction, cumulates from high-MgO melts, or

573 both? *Geology* 41, 67-70.

574 Ackerman, L., Jelínek, E., Medaris Jr., G., Ježek, J., Siebel, W., Strnad, L., 2009.

575 Geochemistry of Fe-rich peridotites and associated pyroxenites from Horní Bory,

576 Bohemian Massif: insights into subduction-related melt-rock reactions. *Chemical*

577 *Geology* 259, 152-167.

578 Anders, E., Ebihara, M., 1982. Solar system abundances of the elements. *Geochimica*

579 *et Cosmochimica Acta* 46, 2363-2380.

580 Arai, S., Ishimaru, S., Mizukami, T., 2012. Methane and propane micro-inclusions in

581 olivine in titanoclinohumite-bearing dunites from the Sanbagawa high-P

582 metamorphic belt, Japan: hydrocarbon activity in a subduction zone and Timobility.

583 *Earth and Planetary Science Letters* 354, 1-11.

584 Arai, S., Yurimoto, H., 1995. Possible sub-arc origin of podiform chromitites. *Island*

585 *Arc* 4, 104-111.

586 Arai, S., Uesugi, J., Ahmed, A.H., 2004. Upper crustal podiform chromitite from the

587 northern Oman ophiolite as the stratigraphically shallowest chromitite in ophiolite

588 and its implication for Cr concentration. *Contributions to Mineralogy and Petrology*

589 147, 145-154.

590 Ballhaus, C., 1998. Origin of podiform chromite deposits by magma mingling. *Earth*

591 *and Planetary Science Letters* 156, 185-193.

592 Ballhaus, C., Berry, R.F., Green, D.H., 1991. High pressure experimental calibration

593 of the olivine-orthopyroxene-spinel oxygen geobarometer: implications for the

594 oxidation state of the upper mantle. *Contributions to Mineralogy and Petrology* 107,

595 27-40.

596 Beattie P., Ford, C., Russell, D., 1991. Partition coefficients for olivine-melt and
597 orthopyroxene-melt systems. *Contributions to Mineralogy and Petrology* 109,
598 212-224.

599 Chan, L.H., Alt, J.C., Teagle, D.A.H., 2002. Lithium and lithium isotope profiles
600 through the upper oceanic crust: a study of seawater-basalt exchange at ODP Sites
601 504B and 896A. *Earth and Planetary Science Letters* 201, 187-201.

602 Chen, C., Su, B.X., Xiao, Y., Pang, K.N., Robinson, P.T., Uysal, İ., Lin, W., Qin, K.Z.,
603 Avcı, E., Kapsiotis, A., 2019. Intermediate chromitite in Kızıldağ ophiolite (SE
604 Turkey) formed during subduction initiation in Neo-Tethys. *Ore Geology Reviews*
605 104, 88-100.

606 Chen, C., Su, B.X., Xiao, Y., Lin, W., Chu, Y., Liu, X., Bai, Y., 2018. Geological
607 records of subduction initiation of Neo-Tethyan ocean: ophiolites and metamorphic
608 soles in southern Turkey. *Acta Petrologica Sinica* 34, 3302-3314 (in Chinese with
609 English abstract).

610 Coogan, L.A., Saunders, A.D., Wilson, R.N., 2014. Aluminum-in-olivine
611 thermometry of primitive basalts: evidence of an anomalously hot mantle source
612 for large igneous provinces. *Chemical Geology* 368, 1-10.

613 De Hoog, J.C.M., Gall, L., Cornell, D.H., 2010. Trace-element geochemistry of
614 mantle olivine and application to mantle petrogenesis and geothermobarometry.
615 *Chemical Geology* 270, 196-215.

616 Derbyshire, E.J., O'Driscoll, B., Lenaz, D., Gertisser, R., Kronz, A., 2013.

617 Compositionally heterogeneous podiform chromitite in the Shetland ophiolite
618 complex (Scotland): Implications for chromitite petrogenesis and late-stage
619 alteration in the upper mantle portion of a supra-subduction zone ophiolite. *Lithos*
620 162, 279-300.

621 Dilek, Y., Thy, P., 2006. Age and petrogenesis of plagiogranite intrusions in the
622 Ankara mélangé, Central Turkey. *Island Arc* 15, 44-57.

623 Elliott, T., Jafcoate, A., Bouman, C., 2004. The terrestrial Li isotope cycles:
624 light-weight constraints on mantle convection. *Earth and Planetary Science Letters*
625 220, 231-245.

626 Foley, S.F., Prelevic, D., Rehfeldt, T., Jacob, D.E., 2013. Minor and trace elements in
627 olivines as probes into early igneous and mantle melting processes. *Earth and*
628 *Planetary Science Letters* 363, 181-191.

629 Foley, S.F., Jacob, D.E., O'Neill, H.S.C., 2011. Trace element variations in olivine
630 phenocrysts from Ugandan potassic rocks as clues to the chemical characteristics of
631 parental magmas. *Contributions to Mineralogy and Petrology* 162, 1-20.

632 Halama, R., Savov, I.P., Rudnick, R.L., McDonough, W.F., 2009. Insights into Li and
633 Li isotope cycling and sub-arc metasomatism from veined mantle xenoliths,
634 Kamcharka. *Contributions to Mineralogy and Petrology* 158, 197-222.

635 Ionov, D.A., Seitz, H.M., 2008. Lithium abundances and isotopic compositions in
636 mantle xenoliths from subduction and intra-plate settings: mantle sources vs.
637 eruption histories. *Earth and Planetary Science Letters* 266, 316-331.

638 Irvine, T.N., Sharpe, M.R., Gallagher, M.L., 1986. Magma mixing and the origin of

639 stratiform oxide ore zones in the Bushveld and Stillwater complexes. *Metallogeny*
640 of Basic and Ultrabasic Rocks, 183-198.

641 Jeffcoate, A.B., Elliott, T., Kasemann, S.A., Ionov, D., Cooper, K., Brooker, R., 2007.
642 Li isotope fractionation in peridotites and mafic melts. *Geochimica et*
643 *Cosmochimica Acta* 71, 202-218.

644 Johnson, C., 2012. Podiform chromite at Voskhod, Kazakhstan. Unpublished PhD
645 Thesis. Cardiff University. <http://orca.cf.ac.uk/40714/>

646 Kamenetsky, V.S., Crawford, A.J., Meffre, S., 2001. Factors controlling chemistry of
647 magmatic spinel: an empirical study of associated olivine, Cr-spinel and melt
648 inclusions from primitive rocks. *Journal of Petrology* 42, 655-671.

649 Lissenberg, C.J., Dick, H.J.B., 2008. Melt-rock reaction in the lower oceanic crust and
650 its implications for the genesis of mid-ocean ridge basalt. *Earth and Planetary*
651 *Science Letters* 271, 311-325

652 Lundstrom, C.C., Chaussidon, M., Hsui, A.T., Kelemen, P., Zimmerman, M., 2005.
653 Observations of Li isotopic variations in the Trinity Ophiolite: evidence for isotopic
654 fractionation by diffusion during mantle melting. *Geochimica et Cosmochimica*
655 *Acta* 69, 735-751.

656 Mazzucchelli, M., Rivalenti, G., Brunelli, D., Zanetti, A., Boari, E., 2009. Formation
657 of highly refractory dunite by focused percolation of pyroxenite-derived melt in the
658 Balmuccia Peridotite Massif (Italy). *Journal of Petrology* 50, 1205-1233.

659 McDonough, W.F., Sun, S.S., 1995. The composition of the Earth. *Chemical Geology*
660 20, 223-253.

661 Oh, C.W., Seo, J., Choi, S.G., Rajesh, V.J., Lee, J.H., 2012. U-Pb SHRIMP zircon
662 geochronology, petrogenesis, and tectonic setting of the Neoproterozoic Baekdong
663 ultramafic rocks in the Hongseong Collision Belt, South Korea. *Lithos* 131,
664 100-112.

665 Paktunc, A.D., 1990. Origin of podiform chromite deposits by multistage melting,
666 melt segregation and magma mixing in the upper mantle. *Ore Geology Reviews* 5,
667 211-222.

668 Pearce, J.A., Barker, P.F., Edward, S.J., Parkinson, I.J., Leat, P.T., 2000. Geochemistry
669 and tectonic significance of peridotites from the south Sandwich arc-basin system,
670 south Atlantic. *Contributions to Mineralogy and Petrology* 139, 36-53.

671 Peighambari, S., Uysal, İ., Stosch, H.G., Ahmadipour, H., Heidarian, H., 2016.
672 Genesis and tectonic settings of ophiolitic chromitites from the Dehsheikh
673 ultramafic complex (Kerman, southeastern Iran): inferences from platinum-group
674 elements and chromite compositions. *Ore Geology Reviews* 74, 39-51.

675 Penniston-Dorland, S., Liu, X.M., Rudnick, R.L., 2017. Lithium isotope geochemistry.
676 *Reviews in Mineralogy and Geochemistry* 82, 165-217.

677 Piccardo, G.B., Zanetti, A., Muntener, O., 2007. Melt/peridotite interaction in the
678 Southern Lanzo peridotite: field, textural and geochemical evidence. *Lithos* 94,
679 181-209.

680 Piccardo, G.B., Muntener, O., Zanetti, A., Pettke, T., 2004. Ophiolitic peridotites of
681 the Alpine-Apennine system: mantle processes and geodynamic
682 relevance. *International Geology Review* 46, 1119-1159.

683 Qian, Q., O'Neill, H.S.C., Hermann, J., 2010. Comparative diffusion coefficients of
684 major and trace elements in olivine ~950°C from a xenocryst included in dioritic
685 magma. *Geology* 4, 331-334.

686 Rampone, E., Borghini, G., Godard, M., Ildefonse, G., Cridpini, L., Fumagalli, P.,
687 2016. Melt/rock reaction at oceanic peridotite/gabbro transition as revealed by trace
688 element chemistry of olivine. *Geochimica et Cosmochimica Acta* 190, 309-331.

689 Reagan, M.K., Pearce, J.A., Petronotis, K., Almeev, R.R., Avery, A.J., Carvalho, C.,
690 Chapman, T., Christeson, G.L., Ferré, E.C., Godard, M., Heaton, D.E., Kirchenbaur,
691 M., Kurz, W., Kutterolf, S., Li, H.Y., Li, Y.B., Michibayashi, K., Morgan, S.,
692 Nelson, W.R., Prytulak, J., Python, M., Robertson, A.H.F., Ryan, J.G., Sager, W.W.,
693 Sakuyama, T., Shervais, J.W., Shimizu, K., Whattam, S.A., 2017. Subduction
694 initiation and ophiolite crust: new insights from IODP drilling. *International*
695 *Geology Review* 59, 1439-1450.

696 Richter, F., Watson, B., Chaussidon, M., Mendybaev, R., Ruscitto, D., 2014. Lithium
697 isotope fractionation by diffusion in minerals. Part I: pyroxenes. *Geochimica et*
698 *Cosmochimica Acta* 126, 352-370.

699 Rollinson, H., Mameri, L., Barry, T., 2018. Polymineralic inclusion in mantle
700 chromitites from the Oman ophiolite indicate a highly magnesian parental melt.
701 *Lithos* 310, 381-391.

702 Rollinson, H., Adetunji, J., 2015. The geochemistry and oxidation state of podiform
703 chromitites from the mantle section of the Oman ophiolite: a review. *Gondwana*
704 *Research* 27, 543-554.

705 Rollinson, H., 2008. The geochemistry of mantle chromitites from the northern part of
706 the Oman ophiolite: inferred parental melt composition. *Contributions to*
707 *Mineralogy and Petrology* 156, 273-288.

708 Rospabé, M., Benoit, M., Ceuleneer, G., Hodel, F., Kaczmarek, M.A., 2018. Extreme
709 geochemical variability through the dunitic transition zone of the Oman ophiolite:
710 implications for melt/fluid reactions at Moho level beneath oceanic spreading
711 centres. *Geochimica Cosmochimica Acta* 234, 1-23.

712 Rudnick, R.L., Ionov, D.A., 2007. Lithium elemental and isotopic disequilibrium in
713 minerals from peridotite xenoliths from far-east Russia: product of recent melt/
714 fluid-rock reaction. *Earth and Planetary Science Letters* 256, 278-293.

715 Sanfilippo, A., Tribuzio, R., Ottolini, L., Hamada, M., 2017. Water, lithium and trace
716 element compositions of olivine from Lanzo South replacive mantle dunite
717 (western Alps): new constraints into melt migration processes at cold thermal
718 regimes. *Geochimica et Cosmochimica Acta* 214, 51-72.

719 Sanfilippo, A., Tribuzio, R., 2011. Melt transport and deformation history in a
720 non-volcanic ophiolitic section northern Apennine, Italy: implications for crustal
721 accretion at slow spreading settings. *Geochemistry, Geophysics, Geosystems* 12,
722 Q0AG04.

723 Santos, J.F., Schärer, U., Ibarra, J.I.G., Girardeau, J., 2002. Genesis of
724 pyroxenite-rich peridotite at Cabo Ortegal (NW Spain): geochemical and Pb-Sr-Nd
725 isotope data. *Journal of Petrology* 43, 17-43.

726 Sarifakioğlu, E., Dilek, Y., Sevin, M., 2017. New synthesis of the
727 Izmir-Ankara-Erzincan suture zone and the Ankara mélangé in northern Anatolia
728 based on new geochemical and geochronological constraints. Geological Society of
729 America Special paper 525, 1-62.

730 Sarifakioğlu, E., Ozen, H., Winchester, J.A., 2009. Whole rock and mineral chemistry
731 of ultramafic-mafic cumulates from the Orhaneli (Bursa) ophiolite, NW Anatolia.
732 Turkish Journal of Earth Sciences 18, 55-83.

733 Seitz, H.M., Woodland, A.B., 2000. The distribution of lithium in peridotitic and
734 pyroxenitic mantle lithologies - an indicator of magmatic and metasomatic
735 processes. Chemical Geology 166, 47-64.

736 Seo, J., Oh, C.W., Choi, S.G., Rajesh, V.J., 2013. Two ultramafic rock types in the
737 Hongseong area, south Korea: tectonic significance for northeast Asia. Lithos 176,
738 30-39.

739 Sobolev, A.V., Hofmann, A.W., Kuzmin, D.V., Yaxley, G.M., Arndt, N.T., Chung, S.L.,
740 Danyushevsky, L.V., Elliott, T., Frey, F.A., Garcia, M.O., Gurenko, A.A.,
741 Kamenetsky, V.S., Kerr, A.C., Krivolutsкая, N.A., Matvienkov, V.V., Nikogosian,
742 I.K., Rocholl, A., Sigurdsson, I.A., Sushchevskaya, N.M., Teklay, M., 2007. The
743 amount of recycled crust in sources of mantle-derived melts. Science 316, 412-417.

744 Song, S.G., Su, L., Niu, Y.L., Zhang, L.F., Zhang, G.B., 2007. Petrological and
745 geochemical constraints on the origin of garnet peridotite in the North Qaidam
746 ultrahigh-pressure metamorphic belt, northwestern China. Lithos 96, 243-265.

747 Stern, R.J., Reagan, M., Ishizuka, O., Ohara, Y., Whattam, S., 2012. To understand
748 subduction initiation, study forearc crust: to understand forearc crust, study
749 ophiolites. *Lithosphere* 4, 469-483.

750 Stosch, H.G., 1981. Sc, Cr, Co and Ni partitioning between minerals from spinel
751 peridotite xenoliths. *Contributions to Mineralogy and Petrology* 78, 166-174.

752 Suhr, G., Hellebrand, E., Snow, J.E., Seck, H.A., Hofmann, A.W., 2003. Significance
753 of large, refractory dunite bodies in the upper mantle of the Bay of Island
754 ophiolite. *Geochemistry, Geophysics, Geosystems* 4.

755 Suhr, G., 1999. Significance of upper mantle hosted dunite bodies for melt migration
756 and extraction under oceanic spreading centres: inferences from reactive transport
757 modelling. *Journal of Petrology* 40, 575-599.

758 Su, B.X., Zhou, M.F., Jing, J.J., Robinson, P., Chen, C., Xiao, Y., Liu, X., Shi, R.D.,
759 Lenaz, D., Hu, Y., 2019. Distinctive melt activity and chromite mineralization in
760 Luobusa and Purang ophiolites, southern Tibet: constraints from trace element
761 compositions of chromite and olivine. *Science Bulletin* 64, 108-121.

762 Su, B.X., Zhou, M.F., Robinson, P.T., 2016. Extremely large fractionation of Li
763 isotopes in a chromitite-bearing mantle sequence. *Scientific Reports* 6, 22370.

764 Su, B.X., Gu, X.Y., Deloule, E., Zhang, H.F., Li, Q.L., Li, X.H., Vigier, N., Tang,
765 Y.J., Tang, G.Q., Liu, Y., Brewer, A., Mao, Q., Ma, Y.G., 2015. Potential
766 orthopyroxene, clinopyroxene and olivine reference materials for in-situ lithium
767 isotope determination. *Geostandards and Geoanalytical Research* 39, 357-369.

768 Su, B.X., Zhang, H.F., Deloule, E., Vigier, N., Hu, Y., Tang, Y.J., Xiao, Y., Sakyi,
769 P.A., 2014. Distinguish silicate and carbonatite mantle metasomatism by using
770 lithium and its isotopes. *Chemical Geology* 381, 67-77.

771 Tankut, A., 1980. The Orhaneli massif, Turkey ophiolites. Geological Survey
772 Department Nicosia, 702-713.

773 Teng, F.Z., McDonough, W.F., Rudnick, R.L., Walker, R.J., Sirbescu, M.L.C., 2006.
774 Lithium isotopic systematics of granites and pegmatites from the Black Hills, South
775 Dakota. *American Mineralogist* 91, 1488-1498.

776 Tomascak, P.B., Magna, T., Dohmen, R., 2016. *Advances in Lithium Isotope*
777 *Geochemistry*. Springer International Publishing Switzerland, 1-195.

778 Tomascak, P.B., Tera, F., Helz, R.T., Walker, R.J., 1999. The absence of lithium
779 isotope fractionation during basalt differentiation: new measurements by
780 multicollector sector ICP-MS. *Geochimica et Cosmochimica Acta* 63, 907-910.

781 Tomascak, P.B., Langmuir, C.H., le Roux, P.J., Shirey, S.B., 2008. Lithium isotopes
782 in global mid-ocean ridge basalts. *Geochimica et Cosmochimica Acta* 72,
783 1626-1637.

784 Tomascak, P.B., Widom, E., Benton, L.D., Goldstein, S.L., Ryan, J.G., 2002. The
785 control of lithium budgets in island arcs. *Earth and Planetary Science Letters* 196,
786 227-238.

787 Uysal, İ., Dokuz, A., Kapsiotis, A., Saka, S., Karşlı, O., Kaliwoda, M., Müller, D.,
788 2017. Petrogenesis of ultramafic rocks from the eastern Orhaneli ophiolite, NW
789 Turkey: hints on the initiation and evolution of melt-peridotite interaction processes

790 within a heterogeneously depleted mantle section. *Journal of Asian Earth*
791 *Sciences* 148, 51-64.

792 Uysal, İ., Akmaz, R.M., Kapsiotis, A., Demir, Y., Saka, S., Avcı, E., Muller, D., 2015.
793 Genesis and geodynamic significance of chromitites from the Orhaneli and
794 Harmancik ophiolites (Bursa, NW Turkey) as evidenced by mineralogical and
795 compositional data. *Ore Geology Reviews* 65, 26-41.

796 Uysal, İ., Şen, A.D., Ersoy, E.Y., Dilek, Y., Saka, S., Zaccarini, F., Escayola, M.,
797 Karlı, O., 2014. Geochemical make-up of oceanic peridotites from NW Turkey
798 and the multi-stage melting history of the Tethyan upper mantle. *Mineralogy and*
799 *Petrology* 108, 49-69.

800 Vlastelic, I., Koga, K., Chauvel, C., Jacques, G., Telouk, P., 2009. Survival of lithium
801 isotopic heterogeneities in the mantle supported by HIMU-lavas from Rurutu Island,
802 Austral Chain. *Earth and Planetary Science Letters* 286, 456-466.

803 Witt-Eickschen, G., O'Neill, H.S.C., 2005. The effect of temperature on the
804 equilibrium distribution of trace elements between clinopyroxene, orthopyroxene,
805 olivine and spinel in upper mantle peridotite. *Chemical Geology* 221, 65-101.

806 Xiao, Y., Teng, F.Z., Su, B.X., Hu, Y., Zhou, M.F., Zhu, B., Shi, R.D., Huang, Q.S.,
807 Gong, X.H. He, Y.S., 2016. Iron and magnesium isotopic constraints on the origin
808 of chemical heterogeneity in podiform chromitite from the Luobusa ophiolite, Tibet.
809 *Geochemistry, Geophysics, Geosystems* 17, 940- 953.

810 Yao, Z.S., Qin, K.Z., Mungall, J.E., 2018. Tectonic controls on Ni and Cu contents of
811 primary mantle-derived magmas for the formation of magmatic sulfide deposits.

812 American Mineralogist 103, 1545-1567.

813 Zhang, P.F., Zhou, M.F., Su, B.X., Uysal, İ., Robinson, P.T., Avcı, E., He, Y.S., 2017.

814 Iron isotopic fractionation and origin of chromitites in the paleo-Moho transition

815 zone of the Kop ophiolite, NE Turkey. *Lithos* 268, 65-75.

816 Zhou, M.F., Robinson, P.T., Su, B.X., Gao, J.F., Li, J.W., Yang, J.S., Malpas, J., 2014.

817 Compositions of chromite, associated minerals, and parental magmas of podiform

818 chromite deposits, the role of slab contamination of asthenospheric melts in

819 suprasubduction zone environments. *Gondwana Research* 26, 262-283.

820 Zhou, M.F., Robinson, P.T., Malpas, J., Edwards, S., Qi, L., 2005. REE and PGE

821 geochemical constraints on the formation of dunites in the Luobusa ophiolite,

822 southern Tibet. *Journal of Petrology* 46, 615-639.

823 Zhou, M.F., Robinson, P.T., Bai, W., 1994. Formation of podiform chromitites by

824 melt/rock interaction in the upper mantle. *Mineralium Deposita* 29, 98-101.

825

826 **Figure Captions:**

827 Fig. 1 (a) Map showing distribution of the continental blocks, major sutures and

828 related ophiolites in the Eastern Mediterranean region (modified after [Chen et al.,](#)

829 [2018](#)). (b) Simplified geological map of the Orhaneli and Harmancık ophiolites (after

830 [Uysal et al., 2015](#)). Red stars in (b) are the sampling locations. IASZ: Izmir-Ankara

831 Suture Zone; ITSZ: Inner-Tauride Suture Zone; BZSZ: Bitlis-Zagros Suture Zone.

832

833 Fig. 2 Photographs of field sites with numbered sampling locations and hand

834 specimens of dunites and chromitites from the Orhaneli mantle-crust transition zone.

835 (a) Banded chromitites that occur by the rhythmic layering of chromitite and dunite.

836 (b) Banded chromitite. (c) Disseminated chromitite.

837

838 Fig. 3 Back scattered electron images of thin sections of dunites and chromitites from

839 the Orhaneli (a)-(c) (sample Ol-1, 2-2 and 4-2) and Harmancık (d) (sample 71.5 m)

840 ophiolites.

841

842 Fig. 4 Plots of (a) MnO vs. Fo of olivine, (b) NiO vs. Fo of olivine, (c) Cr# of

843 chromite vs. Fo, and (d) Cr# vs. TiO₂ of chromite in dunites from the Orhaneli and

844 Harmancık ophiolites. The gray and pink fields represent literature olivine/chromite

845 composition ranges of cumulate dunites and dunites formed by peridotite-melt

846 interaction, respectively. The cumulate dunite field is defined using data from Santos

847 et al. (2002), Song et al. (2007), Arai et al. (2012) and Seo et al. (2013). The replacive

848 dunite field is defined using data from Suhr et al. (2003), Piccardo et al. (2007),

849 Ackerman et al. (2009), Mazzuchelli et al. (2009), Oh et al. (2012), Sanfilippo et al.

850 (2014, 2017).

851

852 Fig. 5 Elemental (Fo, Ni, Mn, Li, Co, Zn, Sc and V) and isotopic ($\delta^7\text{Li}$) variations of

853 olivine compositions in the Orhaneli profile (a) and Harmancık drill hole (b). Olivine

854 grains from dunites are shown as blue circles, whereas pink circles are olivine grains

855 from chromitites. Scanned photographs of dunites and chromitites are shown to

856 clearly describe the effect of chromite proportion on olivine trace element

857 compositions.

858

859 Fig. 6 (a) Primitive mantle-normalized pattern of olivine in the dunites from Orhaneli
860 and Harmancık ophiolites. Plots of (b) Ni (ppm) vs. Mn (ppm), (c) Co (ppm) vs. Mn
861 (ppm) of olivine in the dunites from the two ophiolites. Primitive mantle values are
862 from [Anders and Ebihara \(1982\)](#). Compositions of lower crust data in (a) are from
863 [Sanfilippo et al. \(2014, 2017\)](#) and [Rampone et al. \(2016\)](#). The compositions of olivine
864 phenocrysts in MORB are from [Sobolev et al. \(2007\)](#).

865

866 Fig. 7 Li isotopic compositions of olivines in dunite and chromitites from the Orhaneli
867 and Harmancık ophiolites. The $\delta^7\text{Li}$ range of MORB is from [Tomascak et al. \(2008\)](#),
868 and the $\delta^7\text{Li}$ range of arc lava is from [Tomascak et al. \(2002\)](#) and [Chan et al. \(2002\)](#).

869

870 Fig. 8 Diagram of $\delta^7\text{Li}$ vs. Li of olivine in the Orhaneli and Harmancık dunites. The
871 arrow is the trend of Li diffusion during melt-rock interaction (after [Lundstrom et al.](#)
872 [\(2005\)](#)).

873

874 Fig. 9 A petrologic model for chromitite formation in the Orhaneli and Harmancık
875 ophiolites in the simplified system olivine (Ol) - quartz (Q) - chromite (Chr). The
876 trends in the phase diagrams are after [Zhou et al. \(1994\)](#) and [Zhang et al. \(2017\)](#).

877

878 Fig. 10 (a) TiO_2 vs. Al_2O_3 (after [Kamenetsky et al., 2001](#) and [Derbyshire et al., 2013](#)),

879 (b) Cr# vs. TiO₂ (after [Pearce et al., 2000](#)) of chromite in the chromitites and (c) TiO₂
880 vs. Al₂O₃ (after [Peighambari et al., 2016](#)) of parental melts for the Orhaneli and
881 Harmancık chromitites. FMM: fertile MORB mantle. The subscripts b and I represent
882 boninite and island arc tholeiite, respectively. BON: boninite; IAT: island arc tholeiite;
883 MORB: mid-ocean ridge basalt. Data of grey hexagons, triangles and circles
884 representing lherzolite, harzburgite and dunite, respectively, are from [Uysal et al.](#)
885 [\(2014\)](#).

1 **Formation processes of dunites and chromitites in Orhaneli and Harmancık**
2 **ophiolites (NW Turkey): evidence from in-situ Li isotopes and trace elements in**
3 **olivine**

4

5 Chen Chen^{1,2,3*}, Jan C.M. De Hoog^{4*}, Ben-Xun Su^{1,3,5}, Jing Wang^{1,3,5}, İbrahim Uysal⁶,
6 Yan Xiao^{3,7}

7

8 ¹ Key Laboratory of Mineral Resources, Institute of Geology and Geophysics, Chinese Academy
9 of Sciences, Beijing 100029, China

10 ² Key Laboratory of Mineralogy and Metallogeny, Guangzhou Institute of Geochemistry, Chinese
11 Academy of Sciences, Guangzhou 510460, China

12 ³ Innovation Academy for Earth Science, Chinese Academy of Sciences, Beijing 100029, China

13 ⁴ Grant Institute, School of GeoSciences, The University of Edinburgh, Edinburgh, EH9 3FE,
14 United Kingdom

15 ⁵ University of Chinese Academy of Science, Beijing, 100049, China

16 ⁶ Department of Geological Engineering, Karadeniz Technical University, 61080 Trabzon, Turkey

17 ⁷ State Key Laboratory of Lithospheric Evolution, Institute of Geology and Geophysics, Chinese
18 Academy of Science, Beijing 100029, China

19

20 *Corresponding authors: chenchen2@gig.ac.cn (Chen Chen)

21 ceesjan.dehoog@ed.ac.uk (Jan C.M. De Hoog)

22

23 **Abstract**

24 Trace elements and Li isotopic compositions of olivine from the mantle-crust
25 transition zone of the Bursa ophiolites (including Orhaneli ophiolite and Harmancık
26 ophiolite) in NW Turkey were measured to constrain the genesis of these dunites and
27 chromitites. A cumulate origin for dunite can be ruled out due to the depletion of
28 incompatible trace elements (Zr, Ti, and heavy rare earth elements) in olivine, instead
29 the chemical signatures point to a replacive origin via melt-rock interaction. The
30 olivine grains in the dunites have lower MnO (0.06-0.15 wt.%), Co (106-137 ppm),
31 and higher NiO (0.23-0.44 wt.%) concentrations than olivine phenocrysts in MORB,
32 suggesting these transition-zone dunites have equilibrated with extremely depleted
33 melts. Additionally, the relatively small $\delta^7\text{Li}$ variations of olivine (average $\delta^7\text{Li}$ +4.8
34 to +8.7‰) of the Orhaneli suite indicate the Li isotopic compositions of melts
35 percolating through these dunites are relatively homogeneous. However, the large
36 $\delta^7\text{Li}$ variations of olivine (-2.5 to 20.3‰) in Harmancık dunites can be explained by
37 incomplete diffusive equilibration with melts percolating through these dunites,
38 suggesting infiltration happened not long before obduction of the ophiolite. Olivine in
39 chromitites has higher Fo (92.6-94.7) than coexisting dunites, likely induced by
40 subsolidus Mg-Fe exchange between olivine and chromite. The higher chromite
41 contents of the chromitites can also explain the lower concentrations of Sc, V, Co and
42 Zn in coexisting olivine grains. Mixing of depleted mantle-derived melts and boninitic
43 magmas is suggested to induce a compositional shift from the olivine-chromite
44 cotectic line to the liquidus field of chromite, causing the precipitation of chromite

45 and formation of chromitite layers in the dunites. The heavy Li isotopic compositions
46 (+6 to +11‰) of olivine in chromitites compared to MORB, together with the
47 estimated compositions of parental magmas (Al_2O_3 : 9.8-11.4 wt.%; TiO_2 : 0.22-0.38
48 wt.%) for the chromitites, indicate an arc-like geochemical affinity, hence a
49 subduction-related setting in which these mantle-crust transition zones formed.

50 **Key words:** olivine; trace element; Li isotopes; ophiolite; chromitite; mantle-crust
51 transition zone

52

53 1. Introduction

54 The mantle-crust transition zone is well documented in many ophiolites, and
55 marks the petrological transition from mantle peridotites to lower crustal cumulates
56 (e.g., [Zhang et al., 2017](#); [Rollinson, et al., 2018](#); [Rospabé et al., 2018](#)). Ophiolitic
57 mantle-crust transition zones typically consist of dunite-dominated ultramafic rocks
58 and stratiform-like chromitites, and can reach a thickness of several kilometers
59 ([Paktunc, 1990](#)). These dunites are made of mostly olivine with minor chromite and
60 their thickness ranges from a few meters to a few hundred meters (e.g., [Zhang et al.,](#)
61 [2017](#)). Although the transition zone chromitites are distinguished by their layered
62 morphology from the mantle podiform chromitites which occur as irregular lenses and
63 pods, their compositions are similar in many cases (e.g., [Arai et al., 2004](#); [Rollinson,](#)
64 [2008](#)). Despite many years of investigation, the genesis of the dunites and chromitites
65 in the ophiolitic mantle-crust transition zone is still debated, and different models
66 have been proposed, such as magmatic cumulates stagnating at the base of the crust

67 (e.g., [Abily and Ceuleneer, 2013](#)), crustal assimilation ([Arai et al., 2004](#)), reactions
68 between melts and mantle harzburgites (e.g., [Abily and Ceuleneer, 2013](#)), and mixing
69 of mantle-derived melts with differentiated magmas (e.g., [Ballhaus, 1998](#)). In addition,
70 the nature of the mixed or infiltrated melts and their influences on the mantle-crust
71 transition zone are not yet well known, limiting our understanding of the evolution of
72 ophiolites. A close link between subduction initiation and chromitite/ophiolite genesis
73 has been documented (e.g., [Reagan et al., 2017](#); [Zhang et al., 2017](#)) in several studies
74 of the extensive ophiolites in Turkey (e.g., [Uysal et al., 2017](#); [Chen et al., 2019](#)).
75 Therefore, careful study of the formation processes of the chromitite and their tectonic
76 setting could shine further light on the relationship between subduction initiation and
77 ophiolite emplacement.

78 Olivine is a ubiquitous mineral in both the ultramafic and mafic igneous rocks,
79 and in most cases, it is the first silicate phase to crystallize from ultramafic-mafic
80 melts ([Foley et al., 2013](#)). Olivine thus controls early magmatic differentiation
81 processes, but its Fo content can provide little information about its origin and
82 evolution ([De Hoog et al., 2010](#); [Foley et al., 2013](#)), which forces us to focus on its
83 trace element geochemistry. Consequently, it has become increasingly important to
84 improve our knowledge of the trace element composition of olivine, and to test the
85 use of its geochemical signature as a tracer of early igneous and mantle melting
86 processes ([Foley et al., 2013](#); [Rampone et al., 2016](#)). Several studies have shown that
87 olivines in peridotites from different tectonic environments and/or various origins
88 exhibit distinct geochemical characteristics and define systematic elemental

89 correlations for a series of trace elements (Ni, Mn, Zn, Co, Zr and heavy rare earth
90 elements (HREE)), recording different magmatic processes (Sobolev et al., 2007; De
91 Hoog et al., 2010; Foley et al., 2013; Rampone et al., 2016). Recent work on the
92 Purang and Luobusa ophiolites (Su et al., 2019) advocates that the incompatible trace
93 elements of olivine are more sensitive to melting processes, whereas the
94 concentrations of compatible trace elements are mostly constrained by their source
95 composition.

96 Lithium and its isotopes (^6Li and ^7Li) are increasingly used to trace multiple
97 high-temperature processes due to their moderate incompatibility, strong fluid
98 mobility, and large mass difference (17%) between its two isotopes (e.g., Tomascak et
99 al., 2016). Olivine is the dominant Li reservoir in the upper mantle (Seitz and
100 Woodland, 2000; De Hoog et al., 2010), and olivine-melt partition coefficients of Li
101 are virtually independent of pressure, temperature and olivine composition (Seitz and
102 Woodland, 2000; Qian et al., 2010). The equilibrium fractionation of Li isotopes is
103 likely to be negligible at high temperatures (Vlastelic et al., 2009). However, many
104 natural peridotites display heterogeneous $\delta^7\text{Li}$ compositions, which has been
105 attributed to Li diffusion or interaction between percolating melts and peridotites (e.g.,
106 Lundstrom et al., 2005; Rudnick and Ionov, 2007; Su et al., 2014). Thus, olivine Li
107 isotopic systematics can be used to trace magmatic processes of mantle-crust
108 transition zone dunites and chromitites.

109 In the Bursa ophiolites (Orhaneli and Harmancik ophiolites) in northwestern
110 Turkey, mantle-crust transition zones typically contain interlayered dunites and

111 chromitites (Uysal et al., 2015), the successions of which can reach up a few
112 kilometers thick. In this paper, we provide in-situ trace element and Li isotope
113 analyses of olivine in the chromitites and dunites from the mantle-crust transition
114 zones of Orhaneli and Harmancık ophiolites. These datasets, together with
115 petrological investigations and mineral major oxide compositions, are used to
116 constrain the magmatic processes involved in the formation of dunites and chromitites
117 in ophiolitic mantle-crust transition zones.

118

119 **2. Geological Setting**

120 Tethyan ophiolites in Anatolia occur in several E-W trending belts, which are
121 separated by a series of Gondwana-derived continental fragments (e.g., Uysal et al.,
122 2014) (Fig. 1a). The Izmir-Ankara Suture Zone (IASZ) in northern Turkey occurs
123 between the Sakarya Zone (continent) to the north and the Anatolide-Tauride
124 continental block to the south (Fig. 1a), and has relatively intact ophiolite blocks,
125 which are locally extensive and well preserved (Dilek and Thy, 2006). The Orhaneli
126 and the Harmancık ophiolites, situated in the western part of the IASZ, are considered
127 as remnants of the Izmir-Ankara-Erzincan ocean, a local term for the northern branch
128 of the Neotethys ocean (Sarifakioğlu et al., 2009). The Orhaneli ophiolite was
129 tectonically emplaced onto northwestern Anatolia along the IASZ (Fig. 1a). The
130 Harmancık ophiolite is located ca. 30 km south of the Orhaneli ophiolite (Fig. 1b)
131 (Sarifakioğlu et al., 2009). These two ophiolites were thrust southwards over the
132 metamorphic basement rocks of the Tavşanlı zone in the Anatolide-Tauride platform

133 (Sarifakioğlu et al., 2017).

134 The Orhaneli ophiolite is approximately 50 km long, 15 km wide and 1500 m
135 thick (Fig. 1b; Sarifakioğlu et al., 2009), and mainly consists of mantle-crust
136 transition zone comprising mostly basal ultramafic cumulates. The transition zone is
137 dominated by chromitite interlayered dunites, followed by wehrlites, lherzolites,
138 harzburgites and pyroxenites and to a lesser extent mafic cumulates such as gabbros
139 and gabbronorites (e.g., Sarifakioğlu et al., 2009; Uysal et al., 2015). The chromitites
140 interlayer with dunite in the two ophiolites and have typically semi-massive and
141 banded (stratiform, cumulate) structures (Fig. 2). The mantle-crust transition zone of
142 the Harmancık ophiolite, which reaches up to 1000 m thickness, has similar rock
143 assemblages to those of the Orhaneli ophiolite (Tankut, 1980). The Harmancık
144 ophiolite contains additional podiform chromitites in its mantle section (Sarifakioğlu
145 et al., 2009). The podiform chromitites form centimeters to meters scale
146 lenticular/tabular orebodies enclosed in thick dunite envelopes within mantle
147 harzburgites. The mantle harzburgites and dunites from Harmancık ophiolite have
148 been almost completely altered to serpentine and talc, and are unconformably overlain
149 by Neogene sedimentary units (e.g., Uysal et al., 2014, 2015).

150

151 3. Petrography of dunites and chromitites

152 In the Orhaneli ophiolite, dunites display adcumulate textures and consist of
153 mostly medium- to fine-grained olivine crystals with minor chromites (Fig. 3a, b).
154 Chromitites generally show adcumulus- to orthocumulus-like textures with euhedral

155 to subhedral chromite grains (Fig. 3c). They occur as bands and layers in dunites (Fig.
156 2a-c), and massive chromitites are very rare. The banded chromitite orebodies display
157 schlieren textures, characterized by parallel layers of chromitite alternating with
158 dunite (Fig. 2b). The thickness of the chromitite bands in the Orhaneli ophiolite
159 typically ranges between 0.2 and 3 cm, rarely reaching up to 5 cm (Fig. 2b-c). In
160 contrast, chromitites from the Harmancık mantle-crust transition zone occur as
161 schlieren/bands, semi-massive, and disseminated textures. Chromite grains are mostly
162 euhedral to subhedral. Dunites are made up predominantly of olivine (> 95%) and
163 have a dominant cataclastic texture (Fig. 3d).

164 In the Orhaneli ophiolite, the mantle-crust transition zone is nearly horizontal
165 (Fig. 2a), and we have selected 13 samples (dunites and chromitites) from the
166 mantle-crust transition zone profile. The thickness of this profile is about 90 m and we
167 fixed the base of the dunite as 0 m and its roof is +90 m. In the Harmancık ophiolite,
168 12 drill hole samples from the mantle-crust transition zone were selected for chemical
169 analyses, owing to their pristine olivine grains. The drill hole samples including
170 dunite and chromitite were collected from depths of 63.4 m to 73.4 m.

171

172 **4. Analytical methods**

173 **4.1 Major oxide analysis of minerals**

174 Major oxide compositions of olivine and chromite were determined by
175 wavelength-dispersive X-ray spectrometry using a JEOL JXA8100 electron probe
176 micro-analyzer at the Institute of Geology and Geophysics, Chinese Academy of

177 Sciences (IGGCAS). The analyses were carried out using an accelerating voltage of
178 15 kV, a 10 nA beam current, a 5 μm spot size and 10-30 s peak counting time.
179 Natural and synthetic mineral standards were used for calibration. A ZAF procedure
180 was used for matrix corrections. Typical analytical uncertainty for the analyzed
181 elements was better than 1.5% (1RSD%).

182 **4.2 Trace element analysis of olivine**

183 In-situ trace element analyses of olivine were conducted on thin sections using a
184 laser ablation inductively coupled plasma mass spectrometer (LA-ICP-MS) at
185 IGGCAS. The LA-ICP-MS system consists of a 193 nm Coherent COMPex Pro ArF
186 Excimer laser coupled to an Agilent 7500a ICP-MS. About 6-8 spots were measured
187 for different olivine grains in each sample. The laser spot size was 140 μm , and the
188 repetition rate was 8 Hz. Each analysis consisted of 60 s measurement of gas blank
189 and 60 s ablation. The following isotopes were measured: ^7Li , ^{27}Al , ^{29}Si , ^{31}P , ^{39}K , ^{43}Ca ,
190 ^{45}Sc , ^{49}Ti , ^{51}V , ^{53}Cr , ^{59}Co , ^{66}Zn , ^{91}Zr , ^{163}Dy , ^{166}Er , ^{172}Yb . [De Hoog et al. \(2010\)](#)
191 reported that potential interferences in olivine from matrix components MgO , SiO_2
192 and FeO , which are generated during ablation only and therefore unaccounted for by
193 gas blank subtraction. The contribution of $^{26}\text{Mg}^{40}\text{Ar}$ to the ^{66}Zn signal is about 0.2
194 ppm, and the $^{29}\text{Si}^{16}\text{O}$ interference on ^{45}Sc accounted for 0.2 ppm of the signal ([De](#)
195 [Hoog et al., 2010](#)), hence those are small enough to be ignored. A glass standard,
196 NIST 610, was used for external calibration. For most of the trace elements NIST 612
197 standard was used to monitor instrument drift, and silicon (^{29}Si) was selected as an
198 internal standard. The SiO_2 contents of NIST 610 and NIST 612 are 69.7% and 72.1%,

199 respectively. Reference values of NIST 610 and NIST 612 are from GeoREM
200 (<http://georem.mpch-mainz.gwdg.de>). The data were reduced using the GLITTER 4.0
201 program.

202 **4.3 Li concentration and isotope analyses of olivine**

203 In-situ analyses of Li concentrations and isotopic ratios of olivine were carried
204 out on gold-coated polished thin-sections using a Cameca IMS 1270 SIMS at the
205 Edinburgh Ion Microprobe Facility, in the University of Edinburgh, United Kingdom.
206 A $^{16}\text{O}_2$ primary ion beam with an intensity of 12-16 nA was accelerated to 22.5 kV
207 and impacted onto the sample surface using Kohler illumination. The elliptical spot
208 area was approximately $20 \times 30 \mu\text{m}$. The secondary ion beam position in the field
209 aperture and the ^7Li peak position were automatically centered before each
210 measurement during a 60-s pre-sputter without beam rastering. Secondary ions were
211 counted in mono-collection, pulse-counting mode. Fifty cycles were measured with
212 counting times of 6 and 2.5 s for ^6Li and ^7Li , respectively. The count rate for ^7Li
213 ranged from 30,000 to 120,000 cps, depending on the Li concentration of the sample
214 and primary beam intensity, resulting in 1 s uncertainties of $\delta^7\text{Li}$ of 0.5-1.2‰.
215 Lithium concentrations were calculated using beam current corrected ^7Li count rates
216 of samples using 06JY34O1 as a standard (Li concentration = 1.73 ppm; [Su et al.,](#)
217 [2015](#)). The Li isotopic ratios are expressed as $\delta^7\text{Li}$ relative to the NIST L-SVEC
218 standard $\{\delta^7\text{Li} = [({}^7\text{Li}/{}^6\text{Li})_{\text{sample}}/({}^7\text{Li}/{}^6\text{Li})_{\text{L-SVEC}} - 1] \times 1000\}$. Basaltic standards
219 BCR2-G and ML3B-G were analyzed to monitor instrument drift, whereas 06JY34O1
220 ($\delta^7\text{Li} = 3.1\text{‰}$; [Su et al., 2015](#)) was used for calibration. Matrix composition (Fo

221 content) has an effect on measured olivine Li isotopic compositions; e.g., [Su et al.](#)
222 (2015) showed that $\delta^7\text{Li}$ values increase by 1.0‰ for each mole percent decrease in
223 the Fo content of olivine, and this was taken into account for calibration. As Fo
224 contents of the olivines span a narrow range from 91.6 to 94.7, the matrix correction
225 amounted to no more than 3‰, compared to a range of > 20‰ in $\delta^7\text{Li}$ for the whole
226 dataset.

227

228 **5. Results**

229 **5.1 Major oxide contents of minerals**

230 Olivine in the Orhaneli and Harmancık dunites has Fo values of 92.4-94.0 and
231 91.6-93.5, respectively ([Table S1](#); [Fig. 4a-c](#)). The chromitites contain olivine with
232 somewhat higher Fo values (92.6-94.7 in Orhaneli; 93.3-94.4 in Harmancık) than
233 those in the dunites ([Table S1](#)). The dunites from the two ophiolites have similar MnO
234 (0.06-0.15 wt.%) and NiO (0.23-0.44 wt.%) contents in their olivine ([Table S1](#)). In the
235 Orhaneli and Harmancık profile analyses, the variations of Mn concentrations in
236 olivines are not continuous and yield abrupt change at the contact with chromitite
237 layers. Compared to Mn, Ni concentrations show the reverse patterns ([Fig. 5](#)).

238 Chromite grains in dunites of the both ophiolites are generally uniform in TiO_2
239 contents (0.14-0.23 wt.% in Orhaneli; 0.11-0.22 wt.% in Harmancık), similar to those
240 in the chromitites (0.14-0.26 wt.% and 0.13-0.22 wt.%), whereas their Cr# ($100 \times$
241 $\text{Cr}/(\text{Cr}+\text{Al})$) and Mg# ($100 \times \text{Mg}/(\text{Mg}+\text{Fe})$) values are variable within ranges of
242 79.1-81.8 and 47.6-53.5 in the Orhaneli dunites, 70.6-80.2 and 41.9-52.9 in the

243 Harmancık dunites, 81.1-82.8 and 58.7-67.3 in the Orhaneli chromitites and 78.8-80.0
244 and 46.4-64.2 in the Harmancık chromitites (Table S2; Fig. 4).

245 **5.2 Trace element compositions of olivine**

246 From base to top, the mantle-crust transition zone in the Orhaneli ophiolite
247 includes many cyclic dunite and chromitite layers (Fig. 2a-b) with a total thickness of
248 90 m. Overall, olivines in chromitites show lower Co, Zn, Sc and V concentrations
249 than those in dunites (Fig. 5a, b). The Co concentrations of olivine in the dunites
250 (106-132 ppm in Orhaneli, 128-137 ppm in Harmancık) are higher than those of
251 primitive mantle (105 ppm; McDonough and Sun, 1995), whereas the concentrations
252 of Zn (6.0-44.8 ppm), Sc (2.14-3.68 ppm) and V (0.07-0.36 ppm) in all samples are
253 lower than primitive mantle (Zn: 55 ppm; Sc: 16.2 ppm; V: 82 ppm; McDonough and
254 Sun, 1995). The olivine in both dunites and chromitites from the two ophiolites has
255 lower incompatible trace element concentrations (Ti = 4.0-7.8 ppm, Zr = 0.010-0.034
256 ppm, and Yb = 0.007-0.027 ppm) than the counterparts in olivine phenocrysts in
257 MORB (Table S3; Fig. 6) (e.g., Piccardo et al., 2007; Foley et al., 2011). In the
258 Orhaneli section and Harmancık drill hole samples, there is no apparent correlation
259 between trace element compositions of olivine and the relative position of the layers
260 (Figs. 5, 6).

261 **5.3 Li concentrations and isotopic compositions**

262 In the Orhaneli dunites, olivine has Li concentrations varying from 0.9 to 1.5
263 ppm, and $\delta^7\text{Li}$ from 3.7 to 11.0‰ (Fig. 7), with no correlation between Li
264 concentrations and Li isotopic compositions (Fig. 8). In contrast, Li concentrations

265 (0.7 to 1.9 ppm) and $\delta^7\text{Li}$ values (-2.5 to 20.3‰) of olivine in the Harmancık dunites
266 vary widely (Table S1), and the $\delta^7\text{Li}$ values are negatively correlated with the Li
267 concentrations (Fig. 8). Most olivine grains in the two ophiolites show little change in
268 Li concentrations and $\delta^7\text{Li}$ values from core to rim (Table S1). Nevertheless, different
269 olivine grains in the same sample from Harmancık can have strongly variable Li
270 isotopic compositions (up to 15‰ difference) (Table S1; Fig. 7). On the other hand,
271 the chromitites from the two ophiolites display Li contents and $\delta^7\text{Li}$ values of olivine
272 with 0.8 to 1.6 ppm and 5.0 to 14.7‰ in Orhaneli and 0.7 to 1.2 ppm and 4.1 to 15.6‰
273 in Harmancık (Table S1; Fig. 7).

274

275 **6. Discussion**

276 Based on trace elements and Li isotopes compositions of olivine in the dunites
277 and chromitites from the mantle-crust transition zones for both ophiolites, we first
278 evaluate the various processes that may account for the observed trace elemental and
279 Li isotope variations, followed by models for the formation of dunites and
280 chromitites.

281 **6.1 Origin of mantle-crust transition zone dunites in the Orhaneli and** 282 **Harmancık ophiolites**

283 Dunite consists almost entirely of olivine and is usually formed by one of three
284 processes (e.g., Su et al., 2016; Yao et al., 2018): 1) ultrahigh-degree partial melting of
285 mantle with nearly all orthopyroxene being exhausted; 2) cumulate dunite left behind
286 by the fractionation and accumulation of abundant olivine from an ultramafic-mafic

287 magma; 3) reaction between silica-undersaturated melt migrating in channels and
288 pyroxene-rich wall rock triggering the formation of replacive dunite.

289 Cumulate dunites are formed via crystal accumulation from magmas and
290 therefore olivine generally has low Fo (88-91) and feature a rapid decrease in the NiO
291 content with decreasing Fo (Santos et al., 2002; Song et al., 2007; Arai et al., 2012;
292 Seo et al., 2013; Su et al., 2016; Rospabé et al., 2018). Moreover, the coexisting
293 chromites show a wide range of Cr# from 15 to 76 as well as high TiO₂ contents (up
294 to 0.8 wt.%) (Santos et al., 2002; Song et al., 2007; Arai et al., 2012; Seo et al., 2013)
295 (Fig. 4a-c). In contrast, olivine in replacive dunites generally has higher Fo values (up
296 to 94), because the high-MgO melts reacting with peridotites convert olivine and
297 pyroxene in peridotite to high-Fo olivine (Rollinson et al., 2018). Besides, no obvious
298 correlation exists between the Fo and NiO of olivine grains within the replacive
299 dunites (Mazzucchelli et al., 2009). In the Orhaneli and Harmancık dunites, olivine
300 has higher Fo (91.6-94.0) and lower MnO contents (0.06-0.15 wt.%) than that from
301 cumulate dunites, while chromites display higher Cr# (79.1-82.8) and lower TiO₂
302 contents (0.14-0.26 wt.%) (Fig. 4c-d). These observations, together with the absence
303 of a clear correlation between Fo and NiO in olivine, demonstrate that the dunites
304 from both ophiolites could not be related to fractional crystallization (Fig. 4b). Instead,
305 all our data fall within the fields of replacive dunites (Fo: 90.4-94.6; MnO of olivine:
306 0.07-0.15 wt.%; Cr# of chromite: 23-89) (Suhr et al., 2003; Piccardo et al., 2007;
307 Ackerman et al., 2009; Mazzucchelli et al., 2009; Oh et al., 2012; Sanfilippo et al.,
308 2014, 2017) (Fig. 4), indicating that these dunites were formed by melt-peridotite

309 interaction rather than have a cumulate origin. Furthermore, although the olivines
310 from these dunites show a good correlation between Ni and Mn, the correlation
311 between Co and Mn is poor (Fig. 6b-c). According to olivine-melt partition
312 coefficients (e.g., Beattie et al., 1991), Co and Ni are compatible in olivine, whereas
313 Mn is incompatible, and hence segregation of olivine from its parental magma should
314 produce a decrease of Co and Ni with increasing Mn (Sanfilippo et al., 2014).
315 However, Co contents in olivine from the Orhaneli and Harmancık dunites are poorly
316 correlated with Mn contents, and therefore incompatible with olivine fractionation
317 and likely to be induced by melt migration.

318 For the Orhaneli and Harmancık ophiolites, the mineralogical and geochemical
319 characteristics of mantle-crust transition zone dunites indicate that they were formed
320 by melt-peridotite interaction: orthopyroxene + melt 1 → olivine + melt 2. In this
321 reaction, melt 1 (reactant) is silica-undersaturated and melt 2 (product) is relatively
322 enriched in SiO₂ and Cr₂O₃ due to progressive melt-rock reaction (e.g., Suhr, 1999;
323 Zhou et al., 2005). Since the majority of all dunites are of refractory chemical nature
324 and not akin to MORB (Figs. 4, 6), we argue that the reactant (melt 1) was highly
325 depleted.

326

327 **6.2 Origin of chromitites of the Orhaneli and Harmancık ophiolites**

328 Olivines in Orhaneli and Harmancık chromitites have somewhat higher Fo than
329 that contained in dunites, which likely implies an additional process for the
330 chromitites. Subsolidus Mg-Fe exchange between olivine and chromite has been

331 usually reported in chromitites (e.g., [Xiao et al., 2016](#)):



333 The Mg diffuses from chromite to olivine and Fe from olivine to chromite. The
334 compositional effect of Fe-Mg exchange on olivine depends on the elemental contents
335 and relative modal abundances of olivine and chromite in the rocks ([Xiao et al., 2016](#)).

336 The Fe-Mg exchange effect on olivine in the dunites is negligible because of the
337 extremely low amount of chromite. Recent studies (e.g., [Qian et al., 2010](#)) reported
338 that despite differences in ionic size and charge, Sc and V diffuse at approximately
339 similar rates to Mg, Fe and other divalent cations (e.g., Co and Zn). Cobalt and Zn are
340 more compatible in chromite than in olivine, with crystal-melt partition coefficients
341 from 8.3 to 2.1, and 7.9 to 3.6, respectively (<https://earthref.org>). Vanadium
342 compatibility decreases in the order of chromite >> pyroxene >> olivine
343 ([Witt-Eickschen and O'Neill et al., 2005](#)). In addition, the partitioning of Sc between
344 chromite and olivine is strongly dependent upon the major element composition of
345 chromite ([Stosch et al., 1981](#)). Thus, as expected, Co, Zn, Sc and V concentrations of
346 olivine in the Orhaneli profile and Harmancık chromitites are lower than those in the
347 associated dunites ([Figs. 5a-b](#)), which points to the relative modal abundances of
348 chromite and olivine being a factor in determining the Sc, V, Co and Zn
349 concentrations in olivine in chromitites ([Xiao et al., 2016](#); [Zhang et al., 2017](#)). For
350 example, in the Orhaneli profile, chromitite sample (+50 m) contains the highest
351 modal amount of chromite and its olivine has the lowest Co, Zn, Sc and V
352 concentrations ([Fig. 5a](#)).

353 Mantle-derived magmas generally have ca. 500 ppm Cr concentrations, whereas
354 the chromites derived from these melts contain 30-50 wt.% Cr₂O₃ (Zhou et al., 2014;
355 Zhang et al., 2017). During the evolution of magmatic systems, the oversaturation of
356 chromite in the magma is an important factor for the formation of chromitite. Addition
357 of silica to magmas has been widely accepted as a means of triggering chromite
358 precipitation, because SiO₂ addition can decrease Cr solubility (Irvine et al., 1986).
359 The increase in silica has been usually attributed to assimilation/reaction of more
360 siliceous materials or magma mixing (e.g., Arai et al., 2004; Zhou et al., 1994, 2014;
361 Zhang et al., 2017). In this regard, chromitites in the Orhaneli and Harmancık
362 mantle-crust transition zones are exclusively associated with dunites, and hence it is
363 unlikely that the oversaturation of chromite was caused by extensive assimilation of
364 siliceous-rich crust. Instead, the oversaturation of chromite induced by magma mixing
365 becomes the most likely scenario here. Mantle-derived mafic magma A rises through
366 the upper mantle and mixes with more Si-rich and Cr-rich magma (e.g., Lissenberg
367 and Dick, 2008), upon which the newly-formed, mixed magma B would move into
368 the field of chromite crystallization (Fig. 9). Additionally, the residual melt (melt 2)
369 following melt-peridotite reaction and orthopyroxene dissolution will also be enriched
370 with Cr and SiO₂ relative to the infiltrating melt (Arai and Yurimoto, 1995).
371 Therefore, it would further facilitate the oversaturation of chromite in the mixed
372 magma (Zhou et al., 1994, 2014; Su et al., 2019), driving crystallization of abundant
373 chromite and forming chromitite layers. Due to precipitation of chromite, mixed
374 magma 'B' would evolve to point 'C', i.e., back to the chromite-olivine cotectic line.

375

376 **6.3 Origin of infiltrating melts**

377 During melt-peridotite interaction, trace elements between minerals and melts
378 can be redistributed. The trace elements of olivine in the Orhaneli and Harmancık
379 dunites do not show any zoning (Tables S1, S3), indicating that they were fully
380 equilibrated with the percolating melts. Since dunites predominantly consist of olivine
381 grains, and other silicate minerals (e.g., pyroxene) are rare or absent, the trace element
382 concentrations of olivine cannot be affected by subsolidus re-equilibration among
383 silicate minerals. Thus, the olivine trace elements can be used to trace the composition
384 of the melt in chemical equilibrium with these crystals. The lower incompatible trace
385 element concentrations (Zr, Ti and HREE) in olivines from the Orhaneli and
386 Harmancık dunites relative to those of the olivines from the lower crustal sections of
387 ophiolites (Sanfilippo et al., 2014) (Fig. 6a) indicate that our dunites are not in
388 equilibrium with a melt derived from the lower oceanic crust. In addition, compared
389 to mantle harzburgites of the Orhaneli and Harmancık ophiolites (chromite Cr#: 43-55;
390 Fo < 91.6) (Uysal et al., 2017), the mantle-crust transition zone dunites have Cr# in
391 chromite of 79-82, NiO in olivine of 0.2-0.4 wt.% and Fo of 91.6-94.0, which are far
392 more refractory. The Mn and Co abundances of olivines in both the Orhaneli and
393 Harmancık dunites are lower than those of olivine phenocrysts within MORB
394 (Sobolev et al., 2007) (Fig. 6b-c), in conjunction with the lower trace-element
395 concentrations relative to primitive mantle (McDonough and Sun, 1995), suggesting
396 that these dunites were equilibrated with melts that are more depleted than MORB

397 (e.g., [Piccardo et al., 2004](#); [Sanfilippo and Tribuzio, 2011](#)).

398 We can use the composition of the chromitites to put further constraints on the
399 composition of its parental melts. In contrast to the incompatible elements, diffusion
400 of compatible elements Cr, Al and Ti out of chromite is negligible ([Abily and
401 Ceuleneer, 2013](#)), because Al and Ti enter olivine and/or serpentine in only very low
402 amounts (e.g., [Kamenetsky et al., 2001](#)). As a consequence, we can use these elements
403 to calculate the composition of equilibrated melts based on chromite compositions.
404 The TiO₂ content of chromite is a key indicator of tectonic setting of where chromitite
405 forms (e.g., [Kamenetsky et al., 2001](#)). The Orhaneli and Harmancık chromites have
406 very low TiO₂, and plot in the arc or boninitic fields ([Fig. 10a-b](#)), suggesting
407 crystallization from low-Ti island arc tholeiitic melts or boninitic melts. In addition,
408 several studies have also shown that chromite compositions in chromitites reflect the
409 composition of their parental melt ([Kamenetsky et al., 2001](#); [Rollinson, 2008](#); [Zhou et
410 al., 2014](#); [Rollinson and Adetunji, 2015](#); [Chen et al., 2019](#)). The following equations
411 were proposed by [Rollinson and Adetunji \(2015\)](#) to more closely reflect the empirical
412 correlations defined by [Kamenetsky et al. \(2001\)](#) and applies to melt with an arc
413 affinity:

414
$$(\text{Al}_2\text{O}_3)_{\text{melt}} = 5.2181 \times \ln(\text{Al}_2\text{O}_3)_{\text{Chr}} - 1.0505 \text{ (Eq. 2)}$$

415
$$(\text{TiO}_2)_{\text{melt}} = 1.0963 \times (\text{TiO}_2)_{\text{Chr}}^{0.7863} \text{ (Eq. 3)}$$

416 The implementation of equations (2) and (3) demonstrates that the melts in
417 equilibrium with chromitite have the following composition: 9.8-10.8 wt.% Al₂O₃ and
418 0.23-0.38 wt.% TiO₂ in Orhaneli, and 10.7-11.4 wt.% Al₂O₃ and 0.22-0.33 wt.% TiO₂

419 in Harmancık. The inferred parental melts of the chromitites from the two ophiolites
420 have similar Al₂O₃ and TiO₂ contents to boninitic melts (Fig. 10c), suggesting that the
421 Orhaneli and Harmancık chromitites possibly originated in a forearc setting during the
422 early stage of subduction. The zigzag pattern (Fig. 5) of the olivine trace element
423 contents in the chromitites from the Orhaneli profile and Harmancık drill hole, in
424 conjunction with the widespread occurrence of interlayered chromitites and dunites,
425 could be the witness of multiple magma replenishments in the mantle-crust transition
426 zone.

427

428 **6.4 Lithium isotope constraints on the origin of Orhaneli and Harmancık** 429 **dunites and chromitites**

430 Due to the highly depleted composition of dunites and chromitites, traditional
431 chemical indicators of tectonic setting can generally not be applied. However, Li
432 isotope systematics of olivine may provide clues about the tectonic setting of the
433 infiltrating melts. High-temperature partial melting is thought to induce negligible Li
434 isotope fractionation (e.g., Tomascak et al., 1999; Ionov and Seitz, 2008) and
435 Jeffcoate et al. (2007) estimated that the $\delta^7\text{Li}$ value of magmas generated by
436 equilibrium melting would be < 0.5‰ different from their source. In addition, most
437 studies have shown that Li isotopes do not fractionate during fractional crystallization
438 of silicate magmas (e.g., Tomascak et al., 1999; Teng et al., 2006). Many studies also
439 demonstrated that diffusion is an important mechanism controlling Li abundances and
440 isotopic distribution (e.g., Su et al., 2014; Tomascak et al., 2016). Lithium

441 concentrations and isotopes do not show core-to-rim zoning in individual olivine
442 grains in most samples of the Orhaneli and Harmancik ophiolites (Table S2), and
443 chromite contains little or no Li (e.g., Jeffcoate et al., 2007; Chen et al., 2019). Thus,
444 the Li isotopic compositions of olivine have not been affected by inter-mineral
445 diffusion. Therefore, the Li isotopic compositions of olivines in the Orhaneli and
446 Harmancik dunites record the history of melt-rock interaction.

447 Compared to typical mantle peridotites with $\delta^7\text{Li}$ values of 2-6‰ and 1.0-1.8
448 ppm Li (Seitz and Woodland, 2000; Su et al., 2014), the olivines from the Orhaneli
449 dunites show a similar range of Li concentrations (0.9-1.5 ppm), but a slightly larger
450 range of $\delta^7\text{Li}$ values (+4.0 to +11.0‰) (Table S1; Figs. 7, 8), offset to higher values.
451 As the samples are relatively homogeneous (1s 0.8-1.7‰ based on multiple olivine
452 analyses in each sample) (Fig. 7) and the olivines are unzoned, these samples likely
453 reached Li isotope equilibrium during rock-melt interaction, and therefore could
454 reflect the composition of the infiltrating melt. Average $\delta^7\text{Li}$ per sample shows a more
455 restricted range from +4.8 to +8.7‰ with 1.1-1.3 ppm Li, suggesting reaction with
456 relatively homogeneous melt batches.

457 The Orhaneli chromitites have somewhat higher $\delta^7\text{Li}$ values (average $\delta^7\text{Li}$ per
458 sample +6.0 to +10.6‰ with 1.0-1.3 ppm), but the two samples with highest $\delta^7\text{Li}$
459 shows considerable heterogeneity (based on multiple olivine analyses in each sample)
460 of > 4-7‰ even though individual olivines are unzoned. Excluding these samples, the
461 range of Orhaneli chromitites is +6.0 to +8.2‰, an even smaller range than the
462 dunites. These Li isotopic characteristics could be attributed to infiltrating melts in a

463 subduction zone setting. Dehydration of altered oceanic crusts during subduction can
464 induce that the Li isotope fractionation generates isotopically heavy-Li fluids and
465 light-Li slab residues (e.g., [Elliott et al., 2004](#); [Penniston-Dorland et al., 2017](#)), but the
466 Li isotopic range of arc lavas (-1 to +12‰) reflects the heterogeneity of the altered
467 oceanic plate and overlying sediments ([Tomascak et al., 2002](#); [Elliott et al., 2004](#)).
468 Mixing of various slab components and re-equilibration with Li already present in the
469 mantle wedge results in arc lavas with $\delta^7\text{Li}$ values that only slightly extend beyond
470 that of MORB. The dominance of $\delta^7\text{Li}$ values in the Orhaneli mantle-crust transition
471 zone that extends well beyond the MORB/mantle peridotite range point to a
472 ubiquitous subducting slab component present in the infiltrating melts. The survival of
473 these signatures suggests that the source of the interacting agent was rather shallow,
474 as Li isotopic signatures will re-equilibrate with ambient mantle at short length and
475 timescales ([Halama et al., 2009](#)). This is consistent with a subduction initiation.

476 Compared to Orhaneli, olivine from the Harmancık dunites shows much larger
477 $\delta^7\text{Li}$ variations of -2.5‰ up to +20.3‰, but also larger sample heterogeneity, with
478 only one sample having a ranging of $\delta^7\text{Li}$ of < 3‰ ([Figs. 7, 8](#)). The Harmancık
479 dunites were considerably more altered than the Orhaneli dunites, but the olivine
480 grains selected for Li isotope analyses were fresh and unzoned, and hence the
481 influences of alteration (such as serpentinization) on $\delta^7\text{Li}$ values between different
482 grains are likely to be small (e.g., [Lundstrom et al., 2005](#)). The larger range of $\delta^7\text{Li}$
483 values in the Harmancık dunite may indicate the infiltrating melts with a wider range
484 of $\delta^7\text{Li}$ values, especially given that the slab-derived fluids and melts have a broad

485 range of compositions and are highly variable from one location to another (Elliott et
486 al., 2004; Yao et al., 2018). However, the heterogeneous distribution of $\delta^7\text{Li}$ in
487 individual samples from the Harmancık dunites and the negative correlation between
488 $\delta^7\text{Li}$ values and Li concentrations is indicative of incomplete diffusive equilibration
489 between olivines and infiltrating melts (Fig. 8) (e.g., Jeffcoate et al., 2007;
490 Penniston-Dorland et al., 2017), which is consistent with the studies of olivine Li
491 isotope of dunite from Trinity ophiolite (Lundstrom et al., 2005) and Luobusa
492 ophiolite (Su et al., 2016). Many studies have demonstrated that ^6Li diffuses about 2-3%
493 faster than ^7Li through melts and minerals (e.g., Lundstrom et al., 2005; Teng et al.,
494 2006). As Li diffuses from percolating melt into olivine, the $\delta^7\text{Li}$ of olivine will
495 become lower at first, but will then increase to higher values until $\delta^7\text{Li}$ equilibrates
496 with that of the infiltrating melt, due to equilibrium partitioning (Lundstrom et al.,
497 2005). During this process, temperature and time are the fundamental parameters that
498 control the efficiency of the isotopic exchange (Tomascak et al., 2016). We, therefore,
499 estimated the equilibration temperatures of the Harmancık and Orhaneli dunites and
500 chromitites based on the Al (Coogan et al., 2014) and Mg-Fe exchange (Ballhaus et
501 al., 1991) between olivine and chromite (Table 1). The Al-in-olivine thermometry
502 results (Coogan et al., 2014) show that the temperature range for Harmancık dunites
503 (933-979°C) is similar to that of the Orhaneli suite (960-993°C), while Mg-Fe
504 exchange temperatures (Ballhaus et al., 1991) are considerably lower: 714-778°C for
505 Orhaneli dunites and 663-755°C for Harmancık dunites. This suggests no significant
506 difference in temperature between Harmancık and Orhaneli ophiolites, so this cannot

507 explain the heterogeneity of the Harmancık samples. The main another factor of
508 diffusion is time. Richter et al. (2014) found that very large lithium isotopic
509 fractionations persisted after the lithium concentration had become effectively
510 homogenized during diffusion process, suggesting that it still takes longer for the
511 isotopic composition to become uniform compared to the time it takes for diffusion to
512 homogenize the total lithium concentration. Thus, if infiltration of melts into the rocks
513 occurred shortly before obduction and exhumation, Li isotopes would not fully
514 equilibrate, and isotope heterogeneity would be preserved during relatively rapid
515 cooling. Heterogeneities in the Harmancık samples could indicate rapid cooling was
516 essential to preserve the observed isotope heterogeneities.

517 In summary, excluding two heterogeneous samples (Fig. 7), the Li isotope
518 signatures of olivine in dunites and chromitites from the Orhaneli ophiolite are likely
519 primary features inherited from their parental melts, with all olivines falling between
520 $\delta^7\text{Li}$ values of +5‰ and +9‰, which is within the range of arc lavas but isotopically
521 heavier than MORB (Fig. 7) (Chan et al., 2002; Tomascak et al., 2002), suggesting an
522 affinity with arc magmatism. The olivine Li isotopic compositions of Harmancık
523 mantle-crust transition zone chromitites are similar to those from Orhaneli, but still,
524 likely have diffusional heterogeneities due to incomplete equilibration between
525 infiltrating melt and olivine. Nevertheless, their average compositions (+6 to +11‰)
526 does suggest a melt source similar to the one that crystallized Orhaneli chromitites.

527 The estimated Al_2O_3 and TiO_2 contents of the parental magmas of chromitites in
528 the two ophiolites are similar to the signatures of boninitic melts. Given that boninitic

529 magmas have been widely found in preserved fore-arcs related to subduction
530 initiation (e.g., [Reagan et al., 2017](#); [Stern et al., 2012](#)), this suggests that the Orhaneli
531 and Harmancık ophiolites possibly originated in a subduction initiation setting, which
532 gives additional support to studies suggesting that these settings represent an ideal
533 environment for forming ophiolites with economically viable chromitite deposits
534 ([Johnson, 2012](#)).

535

536 **7 Conclusions**

537 This study presents in-situ trace elements and Li isotopic compositions of olivine
538 in dunites and chromitites from the Orhaneli and Harmancık mantle-crust transition
539 zone. The following conclusions can be drawn:

- 540 1. Compared to olivine from cumulate dunites, the olivine in the Orhaneli and
541 Harmancık dunites is distinct by higher Ni, lower Mn concentrations and extreme
542 depletion of incompatible trace elements (Ti, Zr and HREE), which are consistent
543 with the formation of dunites driven by interaction of peridotite with depleted
544 melts.
- 545 2. The relatively uniform Li isotopic compositions (+4 to +11‰) of olivines from
546 Orhaneli dunites indicate these samples reached Li isotope equilibrium, and
547 suggest a reaction driven by relatively homogeneous melt batches with a
548 subduction component, whereas the large $\delta^7\text{Li}$ variations (-2.5 to +20.3‰) in
549 olivine from Harmancık dunites reflect incomplete diffusive equilibration during
550 the melt percolation through these dunites.

- 551 3. The formation of chromitites in the mantle-crust transition zone of the two
552 ophiolites was likely triggered by the magma mixing. The calculated Al_2O_3
553 (9.8-11.4 wt.%) and TiO_2 (0.22-0.38 wt.%) contents of the parental magmas of
554 chromitites demonstrate a boninite-like geochemical affinity, i.e., a subduction
555 initiation setting, which is in good agreement with the Li isotopic compositions of
556 their olivines.
- 557 4. In contrast to the dunites, the higher Fo contents of olivine in the chromitites
558 could be caused by the Mg-Fe exchange between olivine and chromite. The lower
559 Sc, V, Co and Zn concentrations of olivine in the chromitites are controlled by the
560 modal abundances of chromite.

561

562 **Acknowledgements**

563 This paper benefited from constructive and detailed comments of two
564 anonymous reviewers, and efficient editorial handling by Xian-Hua Li. This study
565 was supported by the National Natural Science Foundation of China (Grants
566 91755205 and 41772055), and by a Visiting Student grant to Chen Chen from the
567 United Kingdom National Environment Research Council 'Deep Volatiles' program
568 (Grant NE/M000427/1). We thank Wei Lin, Yang Chu and Jie-Jun Jing for the
569 assistance in the field trips in the Kızıldağ.

570 **References**

571 Abily, B., Ceuleneer, G., 2013. The dunitic mantle-crust transition zone in the Oman
572 ophiolite: residue of melt-rock interaction, cumulates from high-MgO melts, or

573 both? *Geology* 41, 67-70.

574 Ackerman, L., Jelínek, E., Medaris Jr., G., Ježek, J., Siebel, W., Strnad, L., 2009.

575 Geochemistry of Fe-rich peridotites and associated pyroxenites from Horní Bory,

576 Bohemian Massif: insights into subduction-related melt-rock reactions. *Chemical*

577 *Geology* 259, 152-167.

578 Anders, E., Ebihara, M., 1982. Solar system abundances of the elements. *Geochimica*

579 *et Cosmochimica Acta* 46, 2363-2380.

580 Arai, S., Ishimaru, S., Mizukami, T., 2012. Methane and propane micro-inclusions in

581 olivine in titanoclinohumite-bearing dunites from the Sanbagawa high-P

582 metamorphic belt, Japan: hydrocarbon activity in a subduction zone and Timobility.

583 *Earth and Planetary Science Letters* 354, 1-11.

584 Arai, S., Yurimoto, H., 1995. Possible sub-arc origin of podiform chromitites. *Island*

585 *Arc* 4, 104-111.

586 Arai, S., Uesugi, J., Ahmed, A.H., 2004. Upper crustal podiform chromitite from the

587 northern Oman ophiolite as the stratigraphically shallowest chromitite in ophiolite

588 and its implication for Cr concentration. *Contributions to Mineralogy and Petrology*

589 147, 145-154.

590 Ballhaus, C., 1998. Origin of podiform chromite deposits by magma mingling. *Earth*

591 *and Planetary Science Letters* 156, 185-193.

592 Ballhaus, C., Berry, R.F., Green, D.H., 1991. High pressure experimental calibration

593 of the olivine-orthopyroxene-spinel oxygen geobarometer: implications for the

594 oxidation state of the upper mantle. *Contributions to Mineralogy and Petrology* 107,

595 27-40.

596 Beattie P., Ford, C., Russell, D., 1991. Partition coefficients for olivine-melt and
597 orthopyroxene-melt systems. *Contributions to Mineralogy and Petrology* 109,
598 212-224.

599 Chan, L.H., Alt, J.C., Teagle, D.A.H., 2002. Lithium and lithium isotope profiles
600 through the upper oceanic crust: a study of seawater-basalt exchange at ODP Sites
601 504B and 896A. *Earth and Planetary Science Letters* 201, 187-201.

602 Chen, C., Su, B.X., Xiao, Y., Pang, K.N., Robinson, P.T., Uysal, İ., Lin, W., Qin, K.Z.,
603 Avcı, E., Kapsiotis, A., 2019. Intermediate chromitite in Kızıldağ ophiolite (SE
604 Turkey) formed during subduction initiation in Neo-Tethys. *Ore Geology Reviews*
605 104, 88-100.

606 Chen, C., Su, B.X., Xiao, Y., Lin, W., Chu, Y., Liu, X., Bai, Y., 2018. Geological
607 records of subduction initiation of Neo-Tethyan ocean: ophiolites and metamorphic
608 soles in southern Turkey. *Acta Petrologica Sinica* 34, 3302-3314 (in Chinese with
609 English abstract).

610 Coogan, L.A., Saunders, A.D., Wilson, R.N., 2014. Aluminum-in-olivine
611 thermometry of primitive basalts: evidence of an anomalously hot mantle source
612 for large igneous provinces. *Chemical Geology* 368, 1-10.

613 De Hoog, J.C.M., Gall, L., Cornell, D.H., 2010. Trace-element geochemistry of
614 mantle olivine and application to mantle petrogenesis and geothermobarometry.
615 *Chemical Geology* 270, 196-215.

616 Derbyshire, E.J., O'Driscoll, B., Lenaz, D., Gertisser, R., Kronz, A., 2013.

617 Compositionally heterogeneous podiform chromitite in the Shetland ophiolite
618 complex (Scotland): Implications for chromitite petrogenesis and late-stage
619 alteration in the upper mantle portion of a supra-subduction zone ophiolite. *Lithos*
620 162, 279-300.

621 Dilek, Y., Thy, P., 2006. Age and petrogenesis of plagiogranite intrusions in the
622 Ankara mélangé, Central Turkey. *Island Arc* 15, 44-57.

623 Elliott, T., Jefcoate, A., Bouman, C., 2004. The terrestrial Li isotope cycles:
624 light-weight constraints on mantle convection. *Earth and Planetary Science Letters*
625 220, 231-245.

626 Foley, S.F., Prelevic, D., Rehfeldt, T., Jacob, D.E., 2013. Minor and trace elements in
627 olivines as probes into early igneous and mantle melting processes. *Earth and*
628 *Planetary Science Letters* 363, 181-191.

629 Foley, S.F., Jacob, D.E., O'Neill, H.S.C., 2011. Trace element variations in olivine
630 phenocrysts from Ugandan potassic rocks as clues to the chemical characteristics of
631 parental magmas. *Contributions to Mineralogy and Petrology* 162, 1-20.

632 Halama, R., Savov, I.P., Rudnick, R.L., McDonough, W.F., 2009. Insights into Li and
633 Li isotope cycling and sub-arc metasomatism from veined mantle xenoliths,
634 Kamcharka. *Contributions to Mineralogy and Petrology* 158, 197-222.

635 Ionov, D.A., Seitz, H.M., 2008. Lithium abundances and isotopic compositions in
636 mantle xenoliths from subduction and intra-plate settings: mantle sources vs.
637 eruption histories. *Earth and Planetary Science Letters* 266, 316-331.

638 Irvine, T.N., Sharpe, M.R., Gallagher, M.L., 1986. Magma mixing and the origin of

639 stratiform oxide ore zones in the Bushveld and Stillwater complexes. *Metallogeny*
640 of Basic and Ultrabasic Rocks, 183-198.

641 Jeffcoate, A.B., Elliott, T., Kasemann, S.A., Ionov, D., Cooper, K., Brooker, R., 2007.
642 Li isotope fractionation in peridotites and mafic melts. *Geochimica et*
643 *Cosmochimica Acta* 71, 202-218.

644 Johnson, C., 2012. Podiform chromite at Voskhod, Kazakhstan. Unpublished PhD
645 Thesis. Cardiff University. <http://orca.cf.ac.uk/40714/>

646 Kamenetsky, V.S., Crawford, A.J., Meffre, S., 2001. Factors controlling chemistry of
647 magmatic spinel: an empirical study of associated olivine, Cr-spinel and melt
648 inclusions from primitive rocks. *Journal of Petrology* 42, 655-671.

649 Lissenberg, C.J., Dick, H.J.B., 2008. Melt-rock reaction in the lower oceanic crust and
650 its implications for the genesis of mid-ocean ridge basalt. *Earth and Planetary*
651 *Science Letters* 271, 311-325

652 Lundstrom, C.C., Chaussidon, M., Hsui, A.T., Kelemen, P., Zimmerman, M., 2005.
653 Observations of Li isotopic variations in the Trinity Ophiolite: evidence for isotopic
654 fractionation by diffusion during mantle melting. *Geochimica et Cosmochimica*
655 *Acta* 69, 735-751.

656 Mazzucchelli, M., Rivalenti, G., Brunelli, D., Zanetti, A., Boari, E., 2009. Formation
657 of highly refractory dunite by focused percolation of pyroxenite-derived melt in the
658 Balmuccia Peridotite Massif (Italy). *Journal of Petrology* 50, 1205-1233.

659 McDonough, W.F., Sun, S.S., 1995. The composition of the Earth. *Chemical Geology*
660 20, 223-253.

661 Oh, C.W., Seo, J., Choi, S.G., Rajesh, V.J., Lee, J.H., 2012. U-Pb SHRIMP zircon
662 geochronology, petrogenesis, and tectonic setting of the Neoproterozoic Baekdong
663 ultramafic rocks in the Hongseong Collision Belt, South Korea. *Lithos* 131,
664 100-112.

665 Paktunc, A.D., 1990. Origin of podiform chromite deposits by multistage melting,
666 melt segregation and magma mixing in the upper mantle. *Ore Geology Reviews* 5,
667 211-222.

668 Pearce, J.A., Barker, P.F., Edward, S.J., Parkinson, I.J., Leat, P.T., 2000. Geochemistry
669 and tectonic significance of peridotites from the south Sandwich arc-basin system,
670 south Atlantic. *Contributions to Mineralogy and Petrology* 139, 36-53.

671 Peighambari, S., Uysal, İ., Stosch, H.G., Ahmadipour, H., Heidarian, H., 2016.
672 Genesis and tectonic settings of ophiolitic chromitites from the Dehsheikh
673 ultramafic complex (Kerman, southeastern Iran): inferences from platinum-group
674 elements and chromite compositions. *Ore Geology Reviews* 74, 39-51.

675 Penniston-Dorland, S., Liu, X.M., Rudnick, R.L., 2017. Lithium isotope geochemistry.
676 *Reviews in Mineralogy and Geochemistry* 82, 165-217.

677 Piccardo, G.B., Zanetti, A., Muntener, O., 2007. Melt/peridotite interaction in the
678 Southern Lanzo peridotite: field, textural and geochemical evidence. *Lithos* 94,
679 181-209.

680 Piccardo, G.B., Müntener, O., Zanetti, A., Pettke, T., 2004. Ophiolitic peridotites of
681 the Alpine-Apennine system: mantle processes and geodynamic
682 relevance. *International Geology Review* 46, 1119-1159.

683 Qian, Q., O'Neill, H.S.C., Hermann, J., 2010. Comparative diffusion coefficients of
684 major and trace elements in olivine ~950°C from a xenocryst included in dioritic
685 magma. *Geology* 4, 331-334.

686 Rampone, E., Borghini, G., Godard, M., Ildefonse, G., Cridpini, L., Fumagalli, P.,
687 2016. Melt/rock reaction at oceanic peridotite/gabbro transition as revealed by trace
688 element chemistry of olivine. *Geochimica et Cosmochimica Acta* 190, 309-331.

689 Reagan, M.K., Pearce, J.A., Petronotis, K., Almeev, R.R., Avery, A.J., Carvallo, C.,
690 Chapman, T., Christeson, G.L., Ferré, E.C., Godard, M., Heaton, D.E., Kirchenbaur,
691 M., Kurz, W., Kutterolf, S., Li, H.Y., Li, Y.B., Michibayashi, K., Morgan, S.,
692 Nelson, W.R., Prytulak, J., Python, M., Robertson, A.H.F., Ryan, J.G., Sager, W.W.,
693 Sakuyama, T., Shervais, J.W., Shimizu, K., Whattam, S.A., 2017. Subduction
694 initiation and ophiolite crust: new insights from IODP drilling. *International*
695 *Geology Review* 59, 1439-1450.

696 Richter, F., Watson, B., Chaussidon, M., Mendybaev, R., Ruscitto, D., 2014. Lithium
697 isotope fractionation by diffusion in minerals. Part I: pyroxenes. *Geochimica et*
698 *Cosmochimica Acta* 126, 352-370.

699 Rollinson, H., Mameri, L., Barry, T., 2018. Polymineralic inclusion in mantle
700 chromitites from the Oman ophiolite indicate a highly magnesian parental melt.
701 *Lithos* 310, 381-391.

702 Rollinson, H., Adetunji, J., 2015. The geochemistry and oxidation state of podiform
703 chromitites from the mantle section of the Oman ophiolite: a review. *Gondwana*
704 *Research* 27, 543-554.

705 Rollinson, H., 2008. The geochemistry of mantle chromitites from the northern part of
706 the Oman ophiolite: inferred parental melt composition. *Contributions to*
707 *Mineralogy and Petrology* 156, 273-288.

708 Rospabé, M., Benoit, M., Ceuleneer, G., Hodel, F., Kaczmarek, M.A., 2018. Extreme
709 geochemical variability through the dunitic transition zone of the Oman ophiolite:
710 implications for melt/fluid reactions at Moho level beneath oceanic spreading
711 centres. *Geochimica Cosmochimica Acta* 234, 1-23.

712 Rudnick, R.L., Ionov, D.A., 2007. Lithium elemental and isotopic disequilibrium in
713 minerals from peridotite xenoliths from far-east Russia: product of recent melt/
714 fluid-rock reaction. *Earth and Planetary Science Letters* 256, 278-293.

715 Sanfilippo, A., Tribuzio, R., Ottolini, L., Hamada, M., 2017. Water, lithium and trace
716 element compositions of olivine from Lanzo South replacive mantle dunite
717 (western Alps): new constraints into melt migration processes at cold thermal
718 regimes. *Geochimica et Cosmochimica Acta* 214, 51-72.

719 Sanfilippo, A., Tribuzio, R., 2011. Melt transport and deformation history in a
720 non-volcanic ophiolitic section northern Apennine, Italy: implications for crustal
721 accretion at slow spreading settings. *Geochemistry, Geophysics, Geosystems* 12,
722 Q0AG04.

723 Santos, J.F., Schärer, U., Ibarra, J.I.G., Girardeau, J., 2002. Genesis of
724 pyroxenite-rich peridotite at Cabo Ortegal (NW Spain): geochemical and Pb-Sr-Nd
725 isotope data. *Journal of Petrology* 43, 17-43.

726 Sarifakioğlu, E., Dilek, Y., Sevin, M., 2017. New synthesis of the
727 Izmir-Ankara-Erzincan suture zone and the Ankara mélangé in northern Anatolia
728 based on new geochemical and geochronological constraints. Geological Society of
729 America Special paper 525, 1-62.

730 Sarifakioğlu, E., Ozen, H., Winchester, J.A., 2009. Whole rock and mineral chemistry
731 of ultramafic-mafic cumulates from the Orhaneli (Bursa) ophiolite, NW Anatolia.
732 Turkish Journal of Earth Sciences 18, 55-83.

733 Seitz, H.M., Woodland, A.B., 2000. The distribution of lithium in peridotitic and
734 pyroxenitic mantle lithologies - an indicator of magmatic and metasomatic
735 processes. Chemical Geology 166, 47-64.

736 Seo, J., Oh, C.W., Choi, S.G., Rajesh, V.J., 2013. Two ultramafic rock types in the
737 Hongseong area, south Korea: tectonic significance for northeast Asia. Lithos 176,
738 30-39.

739 Sobolev, A.V., Hofmann, A.W., Kuzmin, D.V., Yaxley, G.M., Arndt, N.T., Chung, S.L.,
740 Danyushevsky, L.V., Elliott, T., Frey, F.A., Garcia, M.O., Gurenko, A.A.,
741 Kamenetsky, V.S., Kerr, A.C., Krivolutsкая, N.A., Matvienkov, V.V., Nikogosian,
742 I.K., Rocholl, A., Sigurdsson, I.A., Sushchevskaya, N.M., Teklay, M., 2007. The
743 amount of recycled crust in sources of mantle-derived melts. Science 316, 412-417.

744 Song, S.G., Su, L., Niu, Y.L., Zhang, L.F., Zhang, G.B., 2007. Petrological and
745 geochemical constraints on the origin of garnet peridotite in the North Qaidam
746 ultrahigh-pressure metamorphic belt, northwestern China. Lithos 96, 243-265.

747 Stern, R.J., Reagan, M., Ishizuka, O., Ohara, Y., Whattam, S., 2012. To understand
748 subduction initiation, study forearc crust: to understand forearc crust, study
749 ophiolites. *Lithosphere* 4, 469-483.

750 Stosch, H.G., 1981. Sc, Cr, Co and Ni partitioning between minerals from spinel
751 peridotite xenoliths. *Contributions to Mineralogy and Petrology* 78, 166-174.

752 Suhr, G., Hellebrand, E., Snow, J.E., Seck, H.A., Hofmann, A.W., 2003. Significance
753 of large, refractory dunite bodies in the upper mantle of the Bay of Island
754 ophiolite. *Geochemistry, Geophysics, Geosystems* 4.

755 Suhr, G., 1999. Significance of upper mantle hosted dunite bodies for melt migration
756 and extraction under oceanic spreading centres: inferences from reactive transport
757 modelling. *Journal of Petrology* 40, 575-599.

758 Su, B.X., Zhou, M.F., Jing, J.J., Robinson, P., Chen, C., Xiao, Y., Liu, X., Shi, R.D.,
759 Lenaz, D., Hu, Y., 2019. Distinctive melt activity and chromite mineralization in
760 Luobusa and Purang ophiolites, southern Tibet: constraints from trace element
761 compositions of chromite and olivine. *Science Bulletin* 64, 108-121.

762 Su, B.X., Zhou, M.F., Robinson, P.T., 2016. Extremely large fractionation of Li
763 isotopes in a chromitite-bearing mantle sequence. *Scientific Reports* 6, 22370.

764 Su, B.X., Gu, X.Y., Deloule, E., Zhang, H.F., Li, Q.L., Li, X.H., Vigier, N., Tang,
765 Y.J., Tang, G.Q., Liu, Y., Brewer, A., Mao, Q., Ma, Y.G., 2015. Potential
766 orthopyroxene, clinopyroxene and olivine reference materials for in-situ lithium
767 isotope determination. *Geostandards and Geoanalytical Research* 39, 357-369.

768 Su, B.X., Zhang, H.F., Deloule, E., Vigier, N., Hu, Y., Tang, Y.J., Xiao, Y., Sakyi,
769 P.A., 2014. Distinguish silicate and carbonatite mantle metasomatism by using
770 lithium and its isotopes. *Chemical Geology* 381, 67-77.

771 Tankut, A., 1980. The Orhaneli massif, Turkey ophiolites. Geological Survey
772 Department Nicosia, 702-713.

773 Teng, F.Z., McDonough, W.F., Rudnick, R.L., Walker, R.J., Sirbescu, M.L.C., 2006.
774 Lithium isotopic systematics of granites and pegmatites from the Black Hills, South
775 Dakota. *American Mineralogist* 91, 1488-1498.

776 Tomascak, P.B., Magna, T., Dohmen, R., 2016. *Advances in Lithium Isotope*
777 *Geochemistry*. Springer International Publishing Switzerland, 1-195.

778 Tomascak, P.B., Tera, F., Helz, R.T., Walker, R.J., 1999. The absence of lithium
779 isotope fractionation during basalt differentiation: new measurements by
780 multicollector sector ICP-MS. *Geochimica et Cosmochimica Acta* 63, 907-910.

781 Tomascak, P.B., Langmuir, C.H., le Roux, P.J., Shirey, S.B., 2008. Lithium isotopes
782 in global mid-ocean ridge basalts. *Geochimica et Cosmochimica Acta* 72,
783 1626-1637.

784 Tomascak, P.B., Widom, E., Benton, L.D., Goldstein, S.L., Ryan, J.G., 2002. The
785 control of lithium budgets in island arcs. *Earth and Planetary Science Letters* 196,
786 227-238.

787 Uysal, İ., Dokuz, A., Kapsiotis, A., Saka, S., Karşlı, O., Kaliwoda, M., Müller, D.,
788 2017. Petrogenesis of ultramafic rocks from the eastern Orhaneli ophiolite, NW
789 Turkey: hints on the initiation and evolution of melt-peridotite interaction processes

790 within a heterogeneously depleted mantle section. *Journal of Asian Earth*
791 *Sciences* 148, 51-64.

792 Uysal, İ., Akmaz, R.M., Kapsiotis, A., Demir, Y., Saka, S., Avcı, E., Muller, D., 2015.
793 Genesis and geodynamic significance of chromitites from the Orhaneli and
794 Harmancik ophiolites (Bursa, NW Turkey) as evidenced by mineralogical and
795 compositional data. *Ore Geology Reviews* 65, 26-41.

796 Uysal, İ., Şen, A.D., Ersoy, E.Y., Dilek, Y., Saka, S., Zaccarini, F., Escayola, M.,
797 Karlı, O., 2014. Geochemical make-up of oceanic peridotites from NW Turkey
798 and the multi-stage melting history of the Tethyan upper mantle. *Mineralogy and*
799 *Petrology* 108, 49-69.

800 Vlastelic, I., Koga, K., Chauvel, C., Jacques, G., Telouk, P., 2009. Survival of lithium
801 isotopic heterogeneities in the mantle supported by HIMU-lavas from Rurutu Island,
802 Austral Chain. *Earth and Planetary Science Letters* 286, 456-466.

803 Witt-Eickschen, G., O'Neill, H.S.C., 2005. The effect of temperature on the
804 equilibrium distribution of trace elements between clinopyroxene, orthopyroxene,
805 olivine and spinel in upper mantle peridotite. *Chemical Geology* 221, 65-101.

806 Xiao, Y., Teng, F.Z., Su, B.X., Hu, Y., Zhou, M.F., Zhu, B., Shi, R.D., Huang, Q.S.,
807 Gong, X.H. He, Y.S., 2016. Iron and magnesium isotopic constraints on the origin
808 of chemical heterogeneity in podiform chromitite from the Luobusa ophiolite, Tibet.
809 *Geochemistry, Geophysics, Geosystems* 17, 940- 953.

810 Yao, Z.S., Qin, K.Z., Mungall, J.E., 2018. Tectonic controls on Ni and Cu contents of
811 primary mantle-derived magmas for the formation of magmatic sulfide deposits.

812 American Mineralogist 103, 1545-1567.

813 Zhang, P.F., Zhou, M.F., Su, B.X., Uysal, İ., Robinson, P.T., Avcı, E., He, Y.S., 2017.

814 Iron isotopic fractionation and origin of chromitites in the paleo-Moho transition

815 zone of the Kop ophiolite, NE Turkey. *Lithos* 268, 65-75.

816 Zhou, M.F., Robinson, P.T., Su, B.X., Gao, J.F., Li, J.W., Yang, J.S., Malpas, J., 2014.

817 Compositions of chromite, associated minerals, and parental magmas of podiform

818 chromite deposits, the role of slab contamination of asthenospheric melts in

819 suprasubduction zone environments. *Gondwana Research* 26, 262-283.

820 Zhou, M.F., Robinson, P.T., Malpas, J., Edwards, S., Qi, L., 2005. REE and PGE

821 geochemical constraints on the formation of dunites in the Luobusa ophiolite,

822 southern Tibet. *Journal of Petrology* 46, 615-639.

823 Zhou, M.F., Robinson, P.T., Bai, W., 1994. Formation of podiform chromitites by

824 melt/rock interaction in the upper mantle. *Mineralium Deposita* 29, 98-101.

825

826 **Figure Captions:**

827 Fig. 1 (a) Map showing distribution of the continental blocks, major sutures and

828 related ophiolites in the Eastern Mediterranean region (modified after [Chen et al.,](#)

829 [2018](#)). (b) Simplified geological map of the Orhaneli and Harmancık ophiolites (after

830 [Uysal et al., 2015](#)). Red stars in (b) are the sampling locations. IASZ: Izmir-Ankara

831 Suture Zone; ITSZ: Inner-Tauride Suture Zone; BZSZ: Bitlis-Zagros Suture Zone.

832

833 Fig. 2 Photographs of field sites with numbered sampling locations and hand

834 specimens of dunites and chromitites from the Orhaneli mantle-crust transition zone.

835 (a) Banded chromitites that occur by the rhythmic layering of chromitite and dunite.

836 (b) Banded chromitite. (c) Disseminated chromitite.

837

838 Fig. 3 Back scattered electron images of thin sections of dunites and chromitites from

839 the Orhaneli (a)-(c) (sample Ol-1, 2-2 and 4-2) and Harmancık (d) (sample 71.5 m)

840 ophiolites.

841

842 Fig. 4 Plots of (a) MnO vs. Fo of olivine, (b) NiO vs. Fo of olivine, (c) Cr# of

843 chromite vs. Fo, and (d) Cr# vs. TiO₂ of chromite in dunites from the Orhaneli and

844 Harmancık ophiolites. The gray and pink fields represent literature olivine/chromite

845 composition ranges of cumulate dunites and dunites formed by peridotite-melt

846 interaction, respectively. The cumulate dunite field is defined using data from Santos

847 et al. (2002), Song et al. (2007), Arai et al. (2012) and Seo et al. (2013). The replacive

848 dunite field is defined using data from Suhr et al. (2003), Piccardo et al. (2007),

849 Ackerman et al. (2009), Mazzuchelli et al. (2009), Oh et al. (2012), Sanfilippo et al.

850 (2014, 2017).

851

852 Fig. 5 Elemental (Fo, Ni, Mn, Li, Co, Zn, Sc and V) and isotopic ($\delta^7\text{Li}$) variations of

853 olivine compositions in the Orhaneli profile (a) and Harmancık drill hole (b). Olivine

854 grains from dunites are shown as blue circles, whereas pink circles are olivine grains

855 from chromitites. Scanned photographs of dunites and chromitites are shown to

856 clearly describe the effect of chromite proportion on olivine trace element

857 compositions.

858

859 Fig. 6 (a) Primitive mantle-normalized pattern of olivine in the dunites from Orhaneli
860 and Harmancık ophiolites. Plots of (b) Ni (ppm) vs. Mn (ppm), (c) Co (ppm) vs. Mn
861 (ppm) of olivine in the dunites from the two ophiolites. Primitive mantle values are
862 from [Anders and Ebihara \(1982\)](#). Compositions of lower crust data in (a) are from
863 [Sanfilippo et al. \(2014, 2017\)](#) and [Rampone et al. \(2016\)](#). The compositions of olivine
864 phenocrysts in MORB are from [Sobolev et al. \(2007\)](#).

865

866 Fig. 7 Li isotopic compositions of olivines in dunite and chromitites from the Orhaneli
867 and Harmancık ophiolites. The $\delta^7\text{Li}$ range of MORB is from [Tomascak et al. \(2008\)](#),
868 and the $\delta^7\text{Li}$ range of arc lava is from [Tomascak et al. \(2002\)](#) and [Chan et al. \(2002\)](#).

869

870 Fig. 8 Diagram of $\delta^7\text{Li}$ vs. Li of olivine in the Orhaneli and Harmancık dunites. The
871 arrow is the trend of Li diffusion during melt-rock interaction (after [Lundstrom et al.](#)
872 [\(2005\)](#)).

873

874 Fig. 9 A petrologic model for chromitite formation in the Orhaneli and Harmancık
875 ophiolites in the simplified system olivine (Ol) - quartz (Q) - chromite (Chr). The
876 trends in the phase diagrams are after [Zhou et al. \(1994\)](#) and [Zhang et al. \(2017\)](#).

877

878 Fig. 10 (a) TiO_2 vs. Al_2O_3 (after [Kamenetsky et al., 2001](#) and [Derbyshire et al., 2013](#)),

879 (b) Cr# vs. TiO₂ (after Pearce et al., 2000) of chromite in the chromitites and (c) TiO₂
880 vs. Al₂O₃ (after Peighambari et al., 2016) of parental melts for the Orhaneli and
881 Harmancık chromitites. FMM: fertile MORB mantle. The subscripts b and I represent
882 boninite and island arc tholeiite, respectively. BON: boninite; IAT: island arc tholeiite;
883 MORB: mid-ocean ridge basalt. Data of grey hexagons, triangles and circles
884 representing lherzolite, harzburgite and dunite, respectively, are from Uysal et al.
885 (2014).

Figure

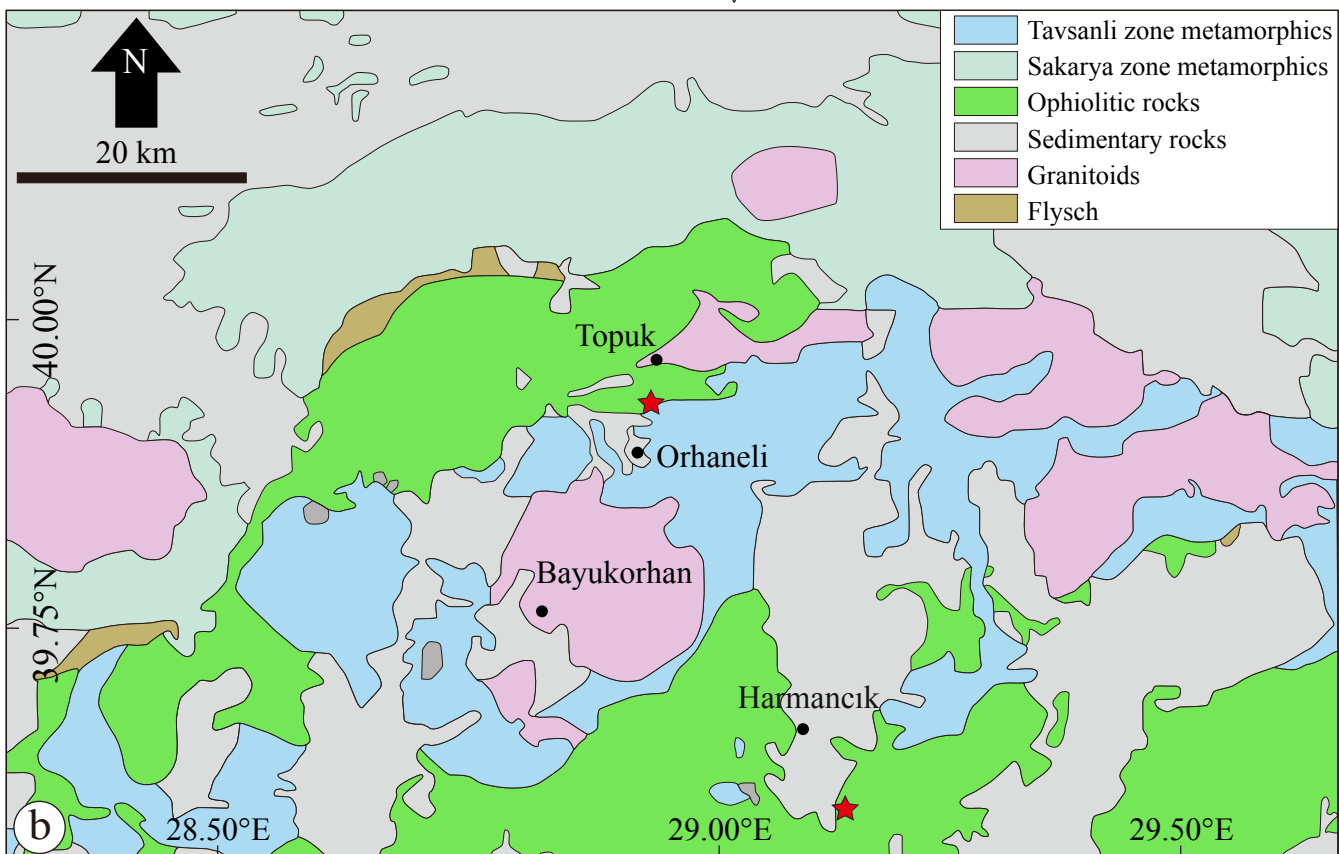
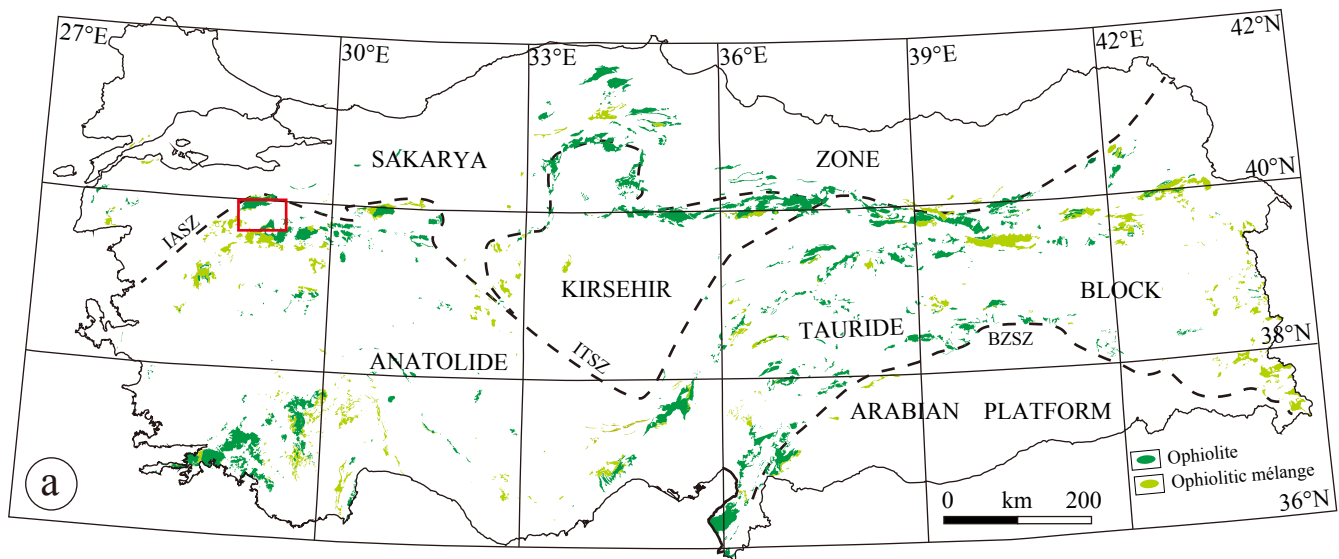


Fig. 1

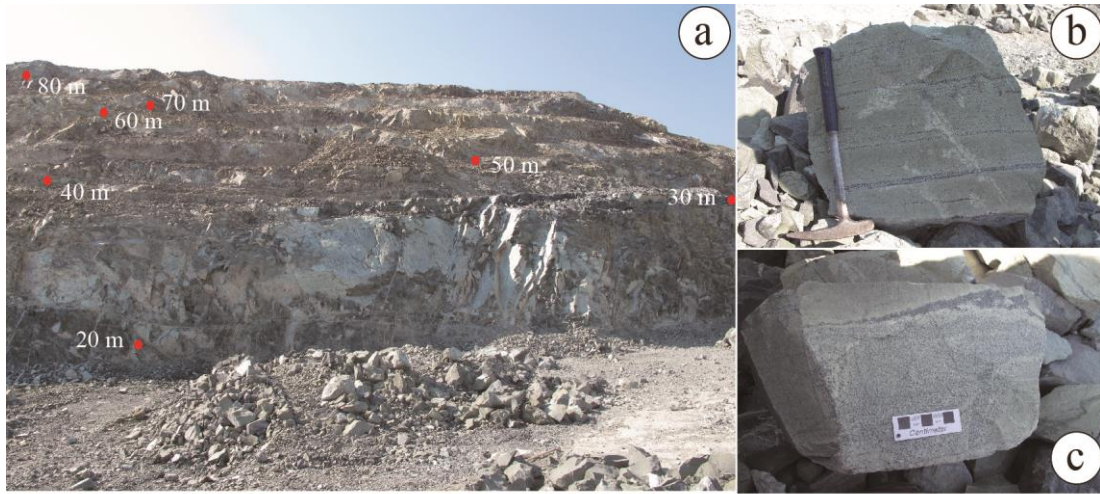


Fig. 2

Figure

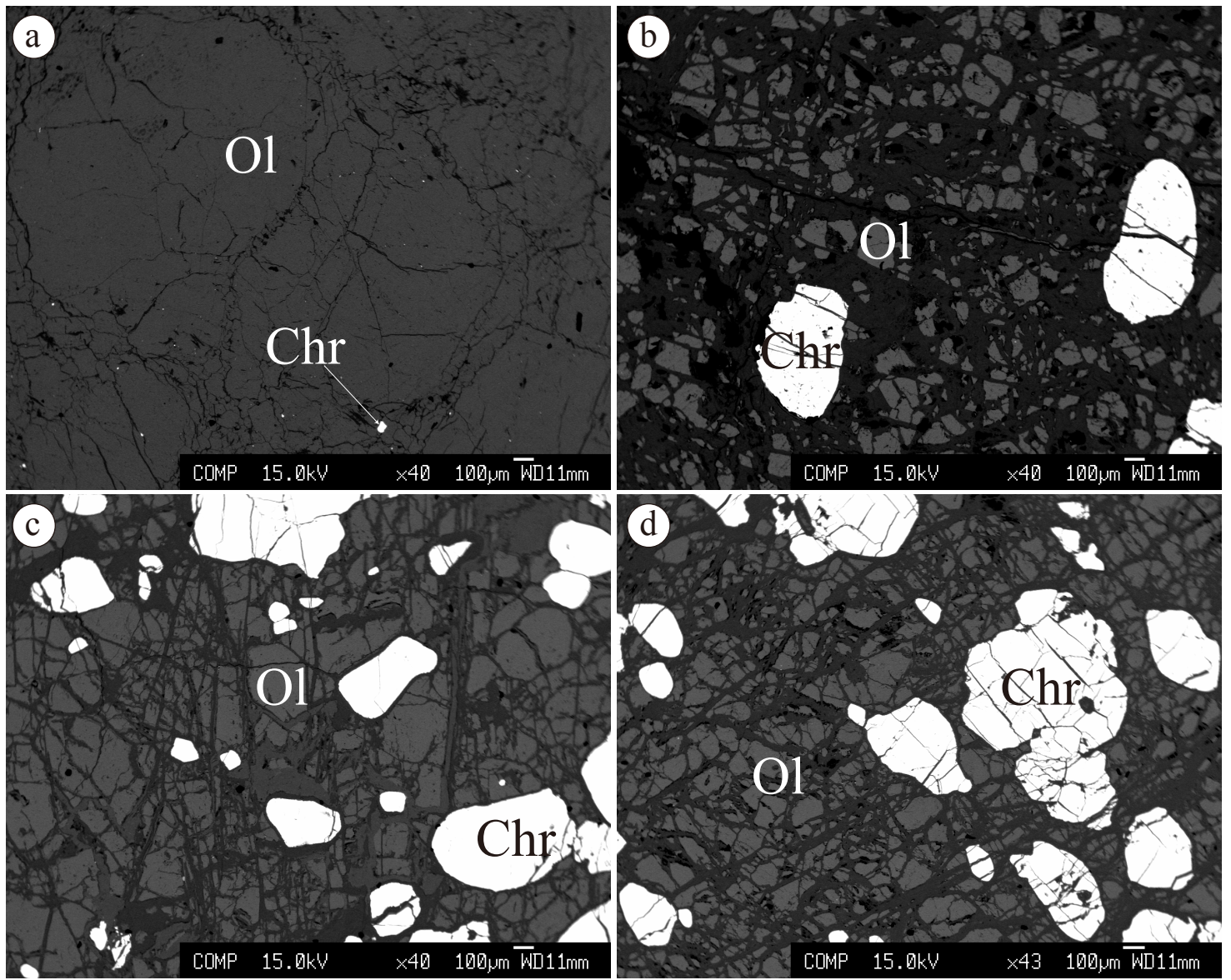


Fig. 3

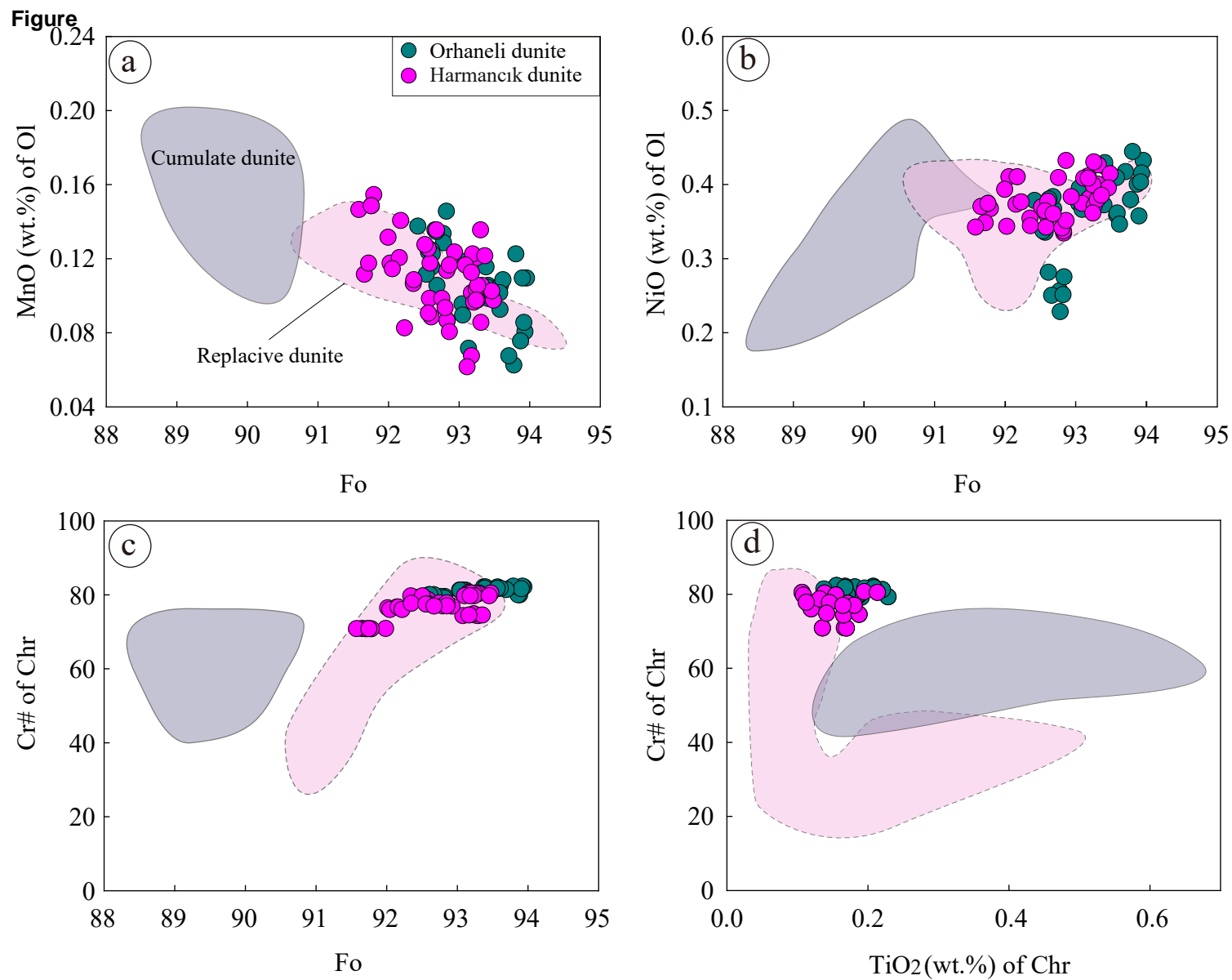


Fig. 4

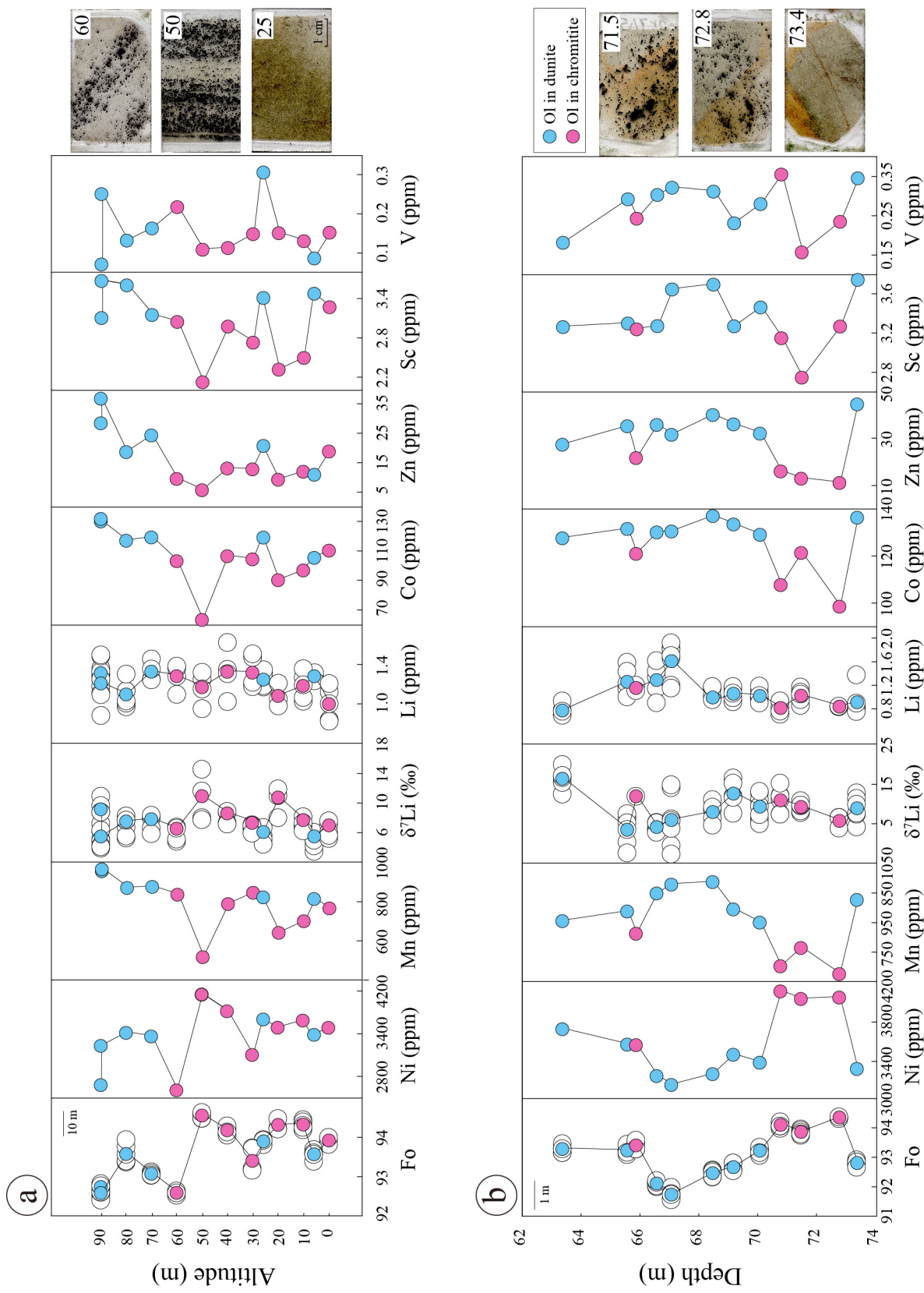


Fig. 5

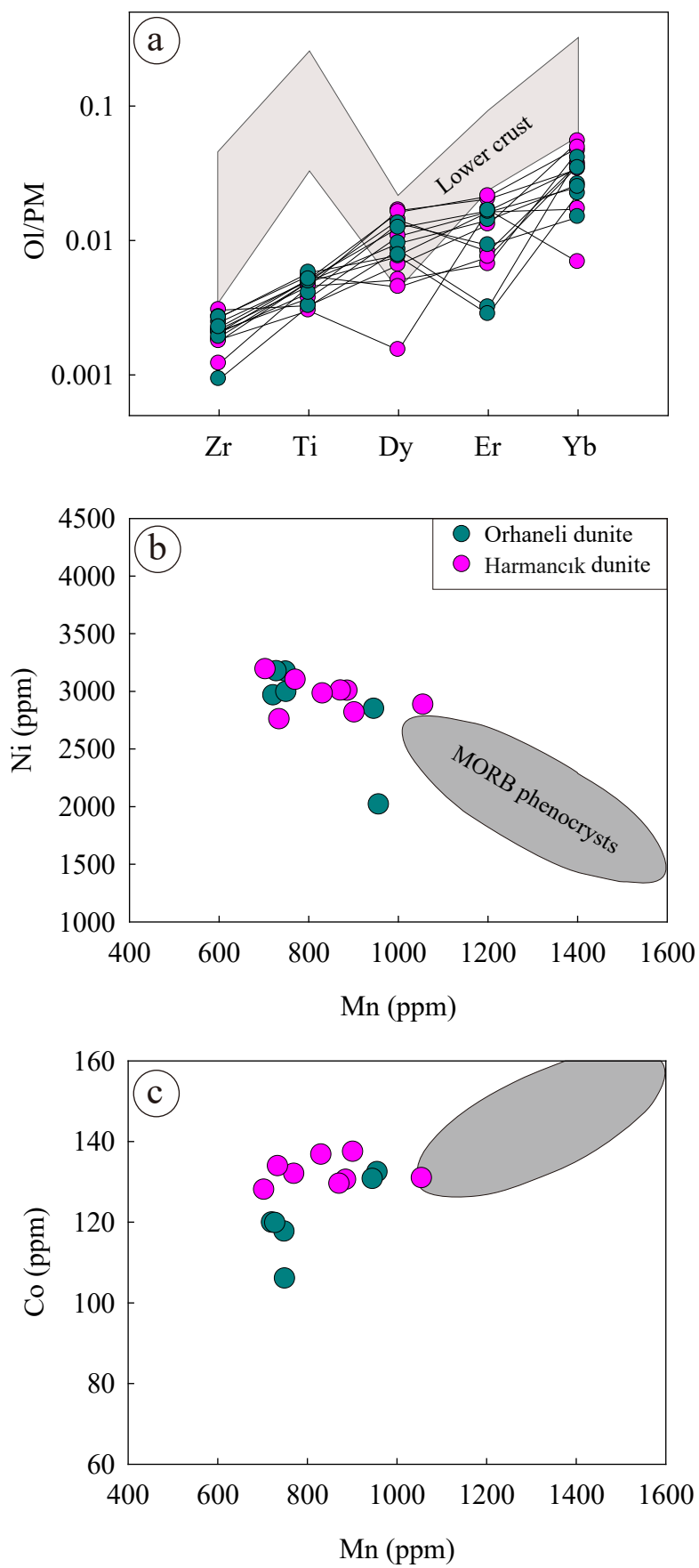


Fig. 6

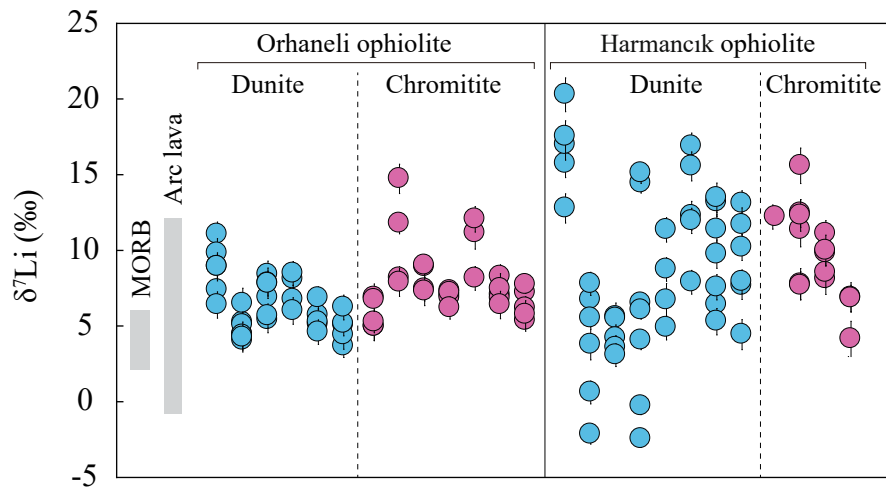


Fig. 7

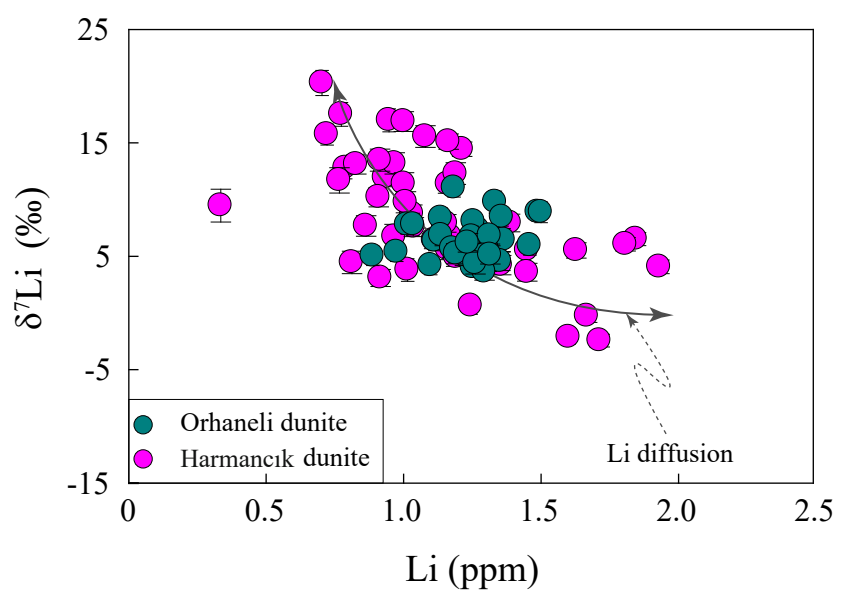


Fig. 8

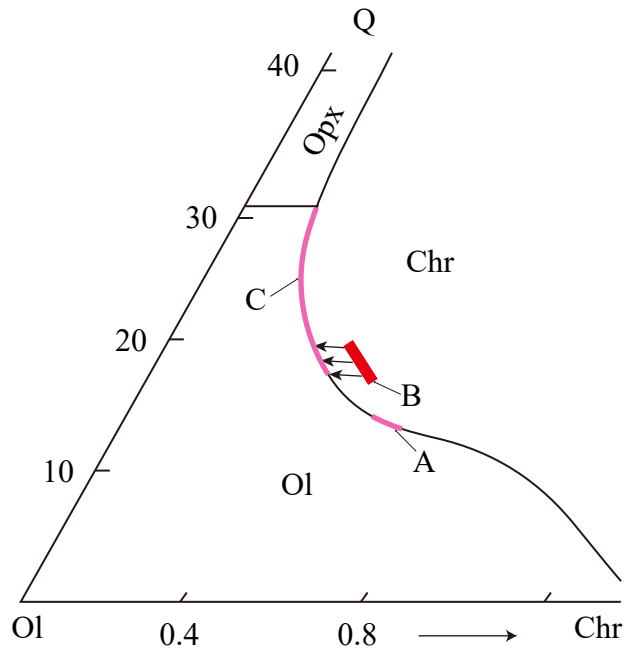


Fig. 9

Figure

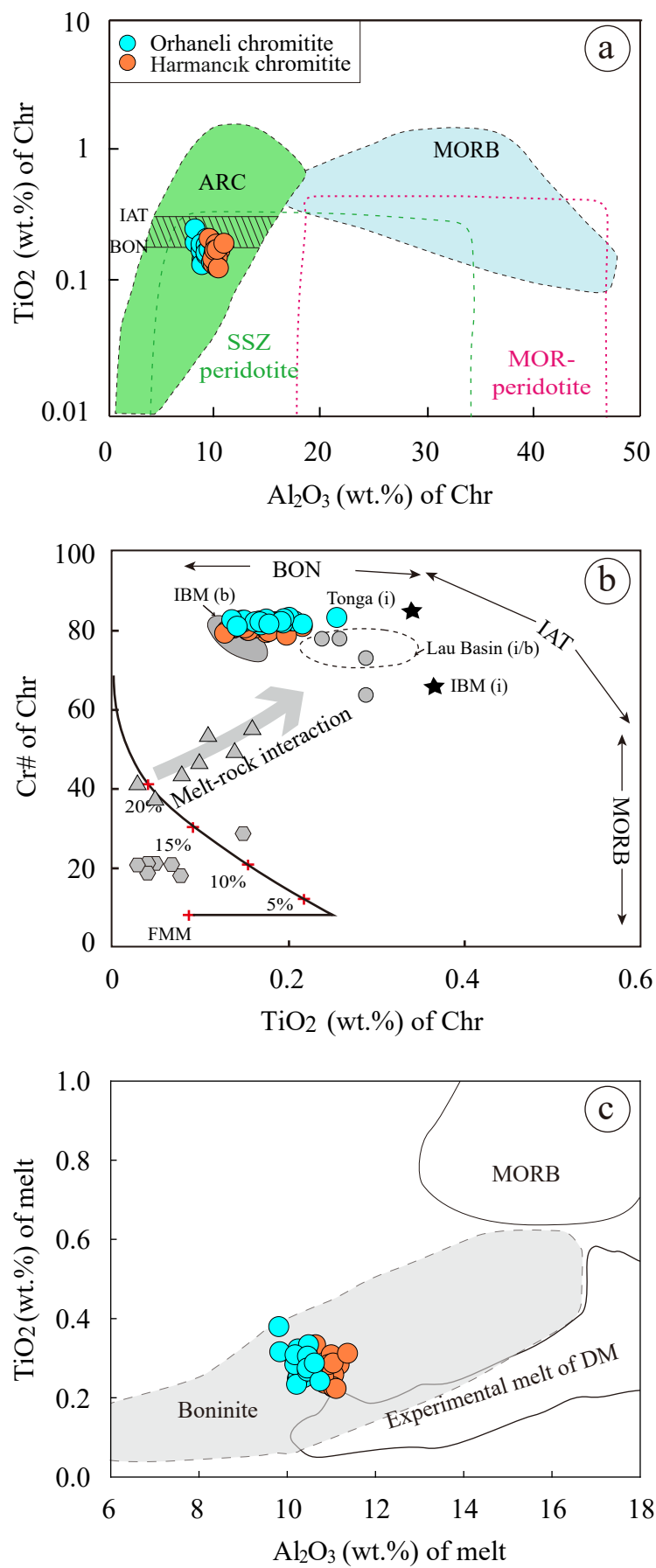


Fig. 10

Table 1. Equilibrium temperature estimates for dunite and chromitite samples from the Orhaneli and Harmancık ophiolites

| | | T(Al-ol) ^a | T Ballhaus (°C) ^b |
|---------------------|------------|-----------------------|------------------------------|
| Orhaneli ophiolite | | | |
| 90 m | Dunite | 967 | 714 |
| 90 m | Dunite | 960 | 724 |
| 80 m | Dunite | 993 | 760 |
| 70 m | Dunite | 974 | 778 |
| 25 m | Dunite | 965 | 720 |
| 5 m | Dunite | 973 | 754 |
| average | | 972 | 742 |
| 60 m | Chromitite | 977 | 754 |
| 50 m | Chromitite | 982 | 828 |
| 40 m | Chromitite | 971 | 779 |
| 30 m | Chromitite | 973 | 863 |
| 20 m | Chromitite | 969 | 840 |
| 10 m | Chromitite | 982 | 839 |
| 0 m | Chromitite | 973 | 940 |
| average | | 975 | 835 |
| Harmancık ophiolite | | | |
| 63.4 m | Dunite | 960 | 755 |
| 65.6 m | Dunite | 979 | 719 |
| 66.6 m | Dunite | 964 | 750 |
| 67.1 m | Dunite | 937 | 691 |
| 68.5 m | Dunite | 953 | 663 |
| 69.2 m | Dunite | 966 | 682 |
| 70.1 m | Dunite | 933 | 690 |
| 73.4 m | Dunite | 972 | 724 |
| average | | 958 | 709 |
| 65.9 m | Chromitite | 985 | 767 |
| 70.8 m | Chromitite | 984 | 858 |
| 71.5 m | Chromitite | 1009 | 744 |
| 72.8 m | Chromitite | 991 | 624 |
| average | | 992 | 748 |

Supplementary material/Appendix (Files for online publication only)

[Click here to download Supplementary material/Appendix \(Files for online publication only\): Data Repository.docx](#)

Conflicts of Interest Statement

Manuscript title: **Formation processes of dunites and chromitites in Orhaneli and Harmancık ophiolites (NW Turkey): evidence from in-situ Li isotopes and trace elements in olivine**

The authors whose names are listed immediately below certify that they have **No** affiliations with or involvement in any organization or entity with any financial interest (Such as honoraria; educational grants; participation in speakers' bureaus; membership, employment, consultancies, stock ownership, or other equity interest; and expert testimony or patent-licensing arrangements), or non-financial interest (such as personal or professional relationship, affiliations, knowledge or beliefs) in the subject matter or materials discussed in this manuscript.

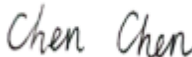

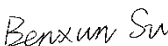
Author names:

Chen Chen, Jan C.M. De Hoog, Ben-Xun Su, Jing Wang, İbrahim Uysal

The authors whose names listed immediately below report the following details of affiliation or involvement in an organization or entity with a financial or non-financial interest in the subject matter or materials discussed in this manuscript. Please specify the nature of the conflict on a separate sheet of paper if the space below is inadequate.

Author names:

This statement is signed by all the authors to indicate agreement that the above information is true and correct:

| Author's name (typed) | Author's signature | Date |
|-----------------------|---|----------------|
| Chen Chen |  | July. 24, 2020 |
| Jan C.M. De Hoog |  | July. 24, 2020 |
| Ben-Xun Su |  | July. 24, 2020 |

Jing Wang

Jing Wang

July. 24, 2020

İbrahim Uysal



July. 24, 2020

Yan Xiao

Yan Xiao

July. 24, 2020